REVIEWS OF GEOPHYSICS AND SPACE PHYSICS, VOL. 20, NO. 4, PAGES 851–875, NOVEMBER 1982

Development of a Turbulence Closure Model for Geophysical Fluid Problems

GEORGE L. MELLOR

Princeton University, Princeton, New Jersey 08540

TETSUJI YAMADA

Los Alamos National Laboratory, Los Alamos, New Mexico 87545

Applications of second-moment turbulent closure hypotheses to geophysical fluid problems have developed rapidly since 1973, when genuine predictive skill in coping with the effects of stratification was demonstrated. The purpose here is to synthesize and organize material that has appeared in a number of articles and add new useful material so that a complete (and improved) description of a turbulence model from conception to application is condensed in a single article. It is hoped that this will be a useful reference to users of the model for application to either atmospheric or oceanic boundary layers.

1. INTRODUCTION

This article is a summary of our experience at Princeton University in second-moment modeling where we have tried to trace model development from the determination of model constants to the applications of the model to geophysical fluid dynamic problems. It includes, in summary fashion, the basic modeling assumptions first put forth by *Mellor and Herring* [1973], *Mellor* [1973], and *Mellor and Yamada* [1974] and references numerous other application papers by us and others who have used the model. New material is also included in this paper.

Our first experience with second-moment turbulence modeling began at the time of the 1968 Stanford Conference on Turbulent Boundary Layer Computation [*Kline et al.*, 1968] with a simple Prandtl type model based on the solution of the turbulent kinetic energy equation. At that time, this model, a model by Bradshaw, and our older eddy viscosity model did very well in predicting all of the data compiled for the conference. Thus it was not clear that more complicated models based on hypotheses by *Rotta* [1951] and *Kolmogorov* [1941] and requiring consideration of all components of the Reynolds stress tensor could be justified on the basis of improving predictions.

The first results from the second-moment calculations of *Donaldson and Rosenbaum* [1968] (using Rotta's energy redistribution hypothesis but not the Kolmogorov isotropic dissipation hypothesis) when applied to wakes and jets and subsequent studies by *Hanjalic and Launder* [1972] were encouraging. The newer models, however, involved more empirical constants than did the older models, which, on this basis alone, would facilitate agreement with data.

Our interest in the Rotta-Kolmogorov model [*Mellor and Herring*, 1973] was greatly enhanced by data obtained by *So and Mellor* [1973, 1975] which demonstrated the effect of wall curvature on turbulent flow. On stable, concave walls the Reynolds stress was virtually extinguished in the inner portion. With no empirical adjustment involving curvature, the model quantitatively predicted this rather dramatic occurrence [*So*, 1975; *Mellor*, 1975]. The same model, when extended in (it now seems) a rather straightforward manner, predicted the observed stabilizing and destabilizing effect of density gradients in a gravity field [*Mellor*, 1973] according to data by *Businger et al.* [1971]. All empirical constants were obtained from neutral flows and were directly related to data for the special case where turbulent energy production is in balance with dissipation. This process of selecting constants is reviewed in this paper and refined somewhat in relation to the earlier papers.

The model was then extended and applied to flows of practical interest in geophysical fluid dynamics. We will illustrate some of these applications and note references to other investigators who have made use of the model.

The model (or models, since there are various degrees of approximation and simplification) is not fundamentally different from models by *Lewellen and Teske* [1973], *Lewellen et al.* [1976], *Launder* [1975], and *Zeman and Lumley* [1976] in that hypotheses by Rotta and Kolmogorov are their more important elements together with the fact that various turbulent length scales, which reside in the hypotheses, are all assumed to be proportional. There are differences. For example, we use a relatively low order version of Rotta's 'energy redistribution' hypothesis. Other authors claim some benefit in adding more nonlinear terms; however, our perception is that the benefits are marginal and may even create errors in one application relative to the one in which the additional, requisite constants were obtained. We also use a fairly simple turbulent diffusion model in contrast, for example, to the more complex diffusion model of *Andre et al.* [1976*a*, *b*]. It is probably true that in many cases, turbulent diffusion is not modeled accurately by us and others. The limiting, free-convection case (a shearless boundary layer heated from below and bounded from above by a stable, inversion layer) is cited by *Lumley et al.* [1978] as an application peculiarly in need of higher-order diffusion modeling. They state that in models using gradient transport, 'the rise of the inversion base is very poorly predicted, while the vertical distribution of turbulent energy is wildly in

Paper number 2R0808.
0034-6853/82/002R-0808$15.00

error.' As will be seen below, our own experience contradicts this statement. As a matter of fact, practically any model, including the so-called 'convective adjustment' model, will produce accurate prediction of the rise of the inversion base, and, further, our model seems to do well in predicting turbulent energy and other turbulent quantities, as did the model by *Lewellen et al.* [1976]. (See also *Lewellen* [1977] for a concise review of the 'ARAP' model. A review by *Harsha* [1977] in the same monograph further reviews a generally simpler class of models.)

The major weakness of all the models probably relates to the turbulent master length scale (or turbulent macroscale, or turbulent inertial scale), and, most important, to the fact that one sets all process scales proportional to a single scale. As we have tried to do here, it is possible first to test the proportionality idea exclusive of the length scale per se, and all seems to work not perfectly, but well.

The master length scale equation we use is quite empirical. It acknowledges that eddies and their scales advect; it undoubtedly interpolates well between the few well-documented laboratory flows on which it is based and does seem to perform correctly for geophysical flows; however, it may be deficient if extrapolated far from its data base. Nevertheless, on conceptual grounds we believe the equation we use is much to be preferred relative to the transport equation for dissipation adopted by many to provide the needed length scale; our reasons will be discussed below.

Although there are differences in the various models, the overall observation may be made that in less than a decade we have progressed from an emphasis on modeling mean flow properties per se to a concern for the accuracy of modeling turbulent variances and covariances. To be more specific, it would appear that in comparison with laboratory data, maximum errors for these latter quantities are of the order of 30–50%, whereas errors in mean properties are much less.

On the basis of the rather broad spectrum of laboratory flows simulated by the models, it may not be too optimistic to believe that they should perform realistically in more complicated geophysical situations. Recent experience where the turbulence models have been incorporated into a large-scale geophysical numerical model contributes to this optimism.

2. The Basic Model

The Closure Assumptions

The equations for the ensemble mean velocity U_i, pressure P, and potential temperature Θ are

$$\frac{\partial \rho}{\partial t} + \frac{\partial}{\partial x_i}(\rho U_i) = 0 \tag{1}$$

$$\rho \frac{DU_j}{Dt} + \rho \varepsilon_{jkl} f_k U_l = \frac{\partial}{\partial x_k}(-\rho \langle u_k u_j \rangle) - \frac{\partial P}{\partial x_j} - g_j \rho \tag{2}$$

$$\rho \frac{D\Theta}{Dt} = \frac{\partial}{\partial x_k}(-\rho \langle u_k \Theta \rangle) \tag{3}$$

where $D(\ )/Dt \equiv U_k \partial(\ )/\partial x_k + \partial(\ )/\partial t$; g_j is the gravity vector, and f_k is the Coriolis vector. Uppercase letters represent ensemble mean variables, whereas lowercase letters are the turbulent variables. Angle brackets represent ensemble means of turbulence variables. An exception is the mean density ρ. It should be noted that the Boussinesq approximation (density a constant except in the buoyancy term) need not be invoked for the mean equations of motion. However, in what follows, the Boussinesq approximation for the turbulence equations is invoked in that density fluctuations are neglected except in the buoyancy term, where, indeed, they exert a profound influence on the turbulence. In the ocean the mean density is related through the equation of state to the mean potential temperature and salinity. The equation for salinity is identical to (3). Analogously, in the atmosphere, mean density is related to mean potential temperature and water vapor. In the following discussion, density fluctuations are written $\beta\theta$, where β is the coefficient of thermal expansion. It is a simple extension to include the effects of salinity and water vapor fluctuation. Inclusion of liquid water in the atmosphere is more complicated and is postponed until section 8.

In general, a radiative flux divergence term should appear on the right side of (3); however, in this paper, radiative effects will not be considered.

If one writes the single-point equations for the moments of velocity and temperature, unknown higher-moment terms appear. The model we adopted [*Mellor and Herring*, 1973; *Mellor*, 1973] (see these papers for the methodology by which the specific tensorial algebra is established) to determine these unknowns is based on the energy redistribution hypothesis of Rotta in the form

$$\left\langle \frac{p}{\rho}\left(\frac{\partial u_i}{\partial x_j} + \frac{\partial u_j}{\partial x_i}\right)\right\rangle = -\frac{q}{3l_1}\left(\langle u_i u_j \rangle - \frac{\delta_{ij}}{3} q^2\right) + C_1 q^2 \left(\frac{\partial U_i}{\partial x_j} + \frac{\partial U_j}{\partial x_i}\right) \tag{4}$$

and the Kolmogorov hypothesis of local, small-scale isotropy such that the dissipation is modeled according to

$$2\nu \left\langle \frac{\partial u_i}{\partial x_k}\frac{\partial u_j}{\partial x_k}\right\rangle = \frac{2}{3}\frac{q^3}{\Lambda_1}\delta_{ij} \tag{5}$$

In the above, u_i is the turbulent fluctuation velocity, whereas $q^2 \equiv \langle u_i^2 \rangle$; p is the fluctuation pressure; ν is the kinematic viscosity; l_1 and Λ_1 are length scales; and C_1 is a nondimensional constant. The above model was then extended [*Mellor*, 1973] to include temperature (or any scalar) such that

$$\left\langle \frac{p}{\rho}\frac{\partial \theta}{\partial x_j}\right\rangle = -\frac{q}{3l_2}\langle u_j \theta \rangle \tag{6}$$

$$(\alpha + \nu)\left\langle \frac{\partial u_j}{\partial x_k}\frac{\partial \theta}{\partial x_k}\right\rangle = 0 \tag{7}$$

where α is the thermal diffusivity. The temperature variance dissipation is

$$2\alpha \left\langle \frac{\partial \theta}{\partial x_k}\frac{\partial \theta}{\partial x_k}\right\rangle = 2\frac{q}{\Lambda_2}\langle \theta^2 \rangle \tag{8}$$

where $\langle \theta^2 \rangle$ is the temperature variance and l_2 and Λ_2 are length scales.

To complete the model, we must add closure expressions for $\langle u_k u_i u_j \rangle$, $\langle p u_j \rangle$, $\langle u_i u_j \theta \rangle$, and $\langle p\theta \rangle$. The choice is ambiguous, as discussed by *Mellor and Herring* [1973] and *Mellor* [1973].

However, we chose

$$\langle u_k u_i u_j \rangle = \tfrac{3}{5}\, lq\, S_q \left(\frac{\partial \langle u_i u_j \rangle}{\partial x_k} + \frac{\partial \langle u_i u_k \rangle}{\partial x_j} + \frac{\partial \langle u_j u_k \rangle}{\partial x_i} \right) \tag{9}$$

$$\langle u_k u_j \theta \rangle = -lq\, S_{u\theta} \left(\frac{\partial \langle u_k \theta \rangle}{\partial x_j} + \frac{\partial \langle u_j \theta \rangle}{\partial x_k} \right) \tag{10}$$

$$\langle u_k \theta^2 \rangle = -lq\, S_\theta \frac{\partial \langle \theta \rangle^2}{\partial x_k} \tag{11}$$

to model what we shall call the turbulent velocity diffusion terms. S_q, $S_{u\theta}$, and S_θ are dimensionless numbers which might be absolute constants or functions of invariant parameters.

Consistent with the above, one might reasonably specify $\langle p\theta \rangle = 0$, since there is no zero-order tensor involving a gradient of a scaler, and also specify $\langle p u_i \rangle = lq\, S_q'\, \partial q^2/\partial x_i$. The problem is that the relative roles of velocity diffusion versus pressure diffusion do not seem to be understood experimentally. However, within approximations made in section 3, the important part of (9) is seen to be $\langle u_k\, u_i^2 \rangle = lq\, S_q\, \partial q^2/\partial x_k$. Thus the pressure and velocity diffusion terms are hardly distinguishable; that is, the present model would probably not discriminate between the two types of diffusion for all of the cases discussed in this paper. To reduce nomenclature, we will here formally set $S_q' = 0$, but it must be stated that we do not know how the model (or, apparently, real data) divides the total diffusion into its two separate parts. There will be more discussion on this point in section 7 relative to the free convection problem.

Despite the uncertainty connected with model equations for turbulent diffusion, it is probable that the concomitant error in predicting mean properties is not large.

It is fundamental to current second-moment models (and, perhaps, their greatest weakness) that all length scales be everywhere proportional to each other. Therefore we set

$$(l_1, \Lambda_1, l_2, \Lambda_2) = (A_1, B_1, A_2, B_2)l \tag{12}$$

where l is the master turbulent length scale. The constants A_1, B_1, A_2, B_2, and C_1 must be determined from data. This can be accomplished without resort to a trial and error process (sometimes termed 'computer optimization') by appealing to data where turbulent energy production and dissipation are balanced. This will be discussed later, as well as means to determine l. The remaining unknowns are S_q, $S_{u\theta}$, and S_θ, although we note here that up to the present time they have been set equal to each other.

Higher-order terms (see definition of 'order' in section 3) can be added to the above closure approximations [*Launder et al.*, 1975; *Launder*, 1975; *Wyngaard*, 1975]: for example, to equation (4) one could add

$$C_2(P_{ikkj} + P_{jkki} - (2\delta_{ij}/3)P_{lkkl}) + C_3(P_{ikjk} + P_{jkik} - (2\delta_{ij}/3)P_{lklk}) + C_4\beta(g_i\langle u_j\theta \rangle + g_j\langle u_i\theta \rangle - (2\delta_{ij}/3)g_k\langle u_k\theta \rangle)$$

where $P_{ijkm} \equiv -\langle u_i u_j \rangle\, \partial U_k/\partial x_m$; to equation (6) one could add

$$C_5 g_j \langle \beta\theta^2 \rangle + C_6 \langle \theta u_k \rangle\, \partial U_k/\partial x_j + C_7 \langle \theta u_k \rangle\, \partial U_j/\partial x_k$$

In a rotating flow, other terms containing the rotation vector can be added along with other higher-order terms [*Lumley and Khajeh-Nouri*, 1974]. Additionally, in the vicinity of walls, terms involving a unit vector λ_i normal to a wall could be included [*Monin*, 1965]. However, we have resisted added complexity for the following reasons: (1) *Mellor* [1973] found that the above model met with immediate success in predicting the very dramatic, stabilizing or destabilizing effects of density stratification in a gravity field. Similar effects of flow curvature were equally well predicted. (2) The data base is not sufficient or accurate enough to determine many constants. (3) We are motivated to minimize complexity and the number of empirical constants. (4) The weakest link in our model (and all other active models) is probably the length scale equation (section 5) rather than the closure assumptions (4)–(11).

Thus the model represented by (4)–(12) is relatively simple. Our expectation of the model is that it will accurately predict mean velocity and temperature fields and do a reasonable job of estimating turbulent variances and covariances.

The Level 4 Model

Now if the closure assumptions are inserted into the mean, turbulent moment equations (contained in many of the references cited in this paper), the model which we had labeled the level 4 model [*Mellor and Yamada*, 1974] is as follows:

$$\frac{D\langle u_i u_j \rangle}{Dt} - \frac{\partial}{\partial x_k}\left[\tfrac{3}{5}\, lq\, S_q \left(\frac{\partial \langle u_i u_j \rangle}{\partial x_k} + \frac{\partial \langle u_i u_k \rangle}{\partial x_j} + \frac{\partial \langle u_j u_k \rangle}{\partial x_i} \right) \right]$$

$$= -\frac{q}{3l_1}\left(\langle u_i u_j \rangle - \frac{\delta_{ij}}{3} q^2 \right) + C_1 q^2 \left(\frac{\partial U_i}{\partial x_j} + \frac{\partial U_j}{\partial x_i} \right) - \frac{2}{3}\frac{q^3}{\Lambda_1}\delta_{ij}$$

$$- \langle u_k u_i \rangle \frac{\partial U_j}{\partial x_k} - \langle u_k u_j \rangle \frac{\partial U_i}{\partial x_k} - \beta(g_j\langle u_i\theta_v \rangle + g_i\langle u_j\theta_v \rangle)$$

$$- f_k(\varepsilon_{jkl}\langle u_l u_i \rangle + \varepsilon_{ikl}\langle u_l u_j \rangle) \tag{13}$$

$$\frac{D\langle u_j\theta \rangle}{Dt} - \frac{\partial}{\partial x_k}\left[lq\, S_{u\theta} \left(\frac{\partial \langle u_j\theta \rangle}{\partial x_k} + \frac{\partial \langle u_k\theta \rangle}{\partial x_j} \right) \right]$$

$$= \langle -u_j u_k \rangle \frac{\partial \Theta}{\partial x_k} - \langle \theta u_k \rangle \frac{\partial U_i}{\partial x_k} - \beta g_j \langle \theta_v \theta \rangle$$

$$- \frac{q}{3l_2}\langle u_j\theta \rangle - f_k \varepsilon_{jkl}\langle u_l\theta \rangle \tag{14}$$

$$\frac{D\langle \theta \rangle^2}{Dt} - \frac{\partial}{\partial x_k}\left[lq\, S_\theta \frac{\partial \langle \theta \rangle^2}{\partial x_k} \right] = -\langle 2u_k\theta \rangle \frac{\partial \Theta}{\partial x_k} - 2\frac{q\langle \theta^2 \rangle}{\Lambda_2} \tag{15}$$

In the above equations we distinguish θ_v from θ where the former always appears in combination with β, thus representing a density fluctuation. However, for most of the discussion in this paper we let $\theta_v = \theta$, in which case the above equation set is closed. Later, however, we will consider atmospheric problems where water vapor and liquid must be included in the equation of state and oceanic problems where salinity is an important factor; then θ_v and θ will acquire separate identities.

3. SIMPLIFIED MODELS

The Level 3 Model

Although we have used the complete model in the numerical solution of problems [*Mellor and Yamada*, 1974, *Briggs et al.*, 1976], it is generally too complicated for practical application to most geophysical fluid dynamics problems. As discussed later, the model must be extended to include other scalar quantities besides temperature (in the atmosphere, water vapor and liquid water along with other chemical constituents; in the oceans, salinity and other chemical constituents), and the numerical effort can quickly get out of hand.

A process of simplification has been described by *Mellor and Yamada* [1974] in some detail. Briefly, it involves scaling all terms in the model equations as a product of q^3/Λ and powers of $\mathbf{a}$, where $\Lambda = O(\Lambda_1)$ and $\mathbf{a}^2 = O(\mathbf{a}_{ij}^2)$; $\mathbf{a}_{ij}$ is the nondimensional measure of anisotropy in the expression

$$\langle u_i u_j \rangle = \left(\frac{\delta_{ij}}{3} + \mathbf{a}_{ij} \right) q^2$$

Similar parameters are introduced for the temperature variables. We then evaluated terms in (13), (14), and (15) in powers of $\mathbf{a}$ and eliminated terms of order $\mathbf{a}^2$. All of this is suggested by the kinetic theory of gases, wherein $\mathbf{a}$ is related to the Knudson number and is generally a very small number. For turbulent flows, $\mathbf{a}_{ij}^2 \simeq 0.15$ and is not overly small. Nevertheless, the procedure contributes some discipline to the process of simplification and provides a self-consistent model. What we have called a 'level 3' model [*Mellor and Yamada*, 1974] is as follows:

$$\frac{Dq^2}{Dt} - \frac{\partial}{\partial x_k}\left[lq\, S_q \frac{\partial q^2}{\partial x_k} \right] = 2(P_s + P_b - \varepsilon) \tag{16}$$

$$\langle u_i u_j \rangle = \frac{\delta_{ij}}{3} q^2 - \frac{3l_1}{q}\left[\langle u_k u_i \rangle \frac{\partial U_j}{\partial x_k} + \langle u_k u_j \rangle \frac{\partial U_i}{\partial x_k} + \tfrac{2}{3}\delta_{ij} P_s \right.$$

$$- C_1 q^2 \left(\frac{\partial U_j}{\partial x_i} + \frac{\partial U_i}{\partial x_j} \right) + \beta g_j \langle u_j \theta_v \rangle + \beta g_i \langle u_j \theta_v \rangle + \tfrac{2}{3}\delta_{ij} P_b$$

$$\left. + f_k(\varepsilon_{jkl}\langle u_l u_i \rangle + \varepsilon_{ikl}\langle u_l u_j \rangle) \right] \tag{17}$$

$$\langle u_j \theta \rangle = -\frac{3l_2}{q}\left[\langle u_j u_k \rangle \frac{\partial \Theta}{\partial x_k} + \langle \theta u_k \rangle \frac{\partial U_j}{\partial x_k} \right.$$

$$\left. + \beta g_j \langle \theta_v \theta \rangle + f_k\, \varepsilon_{jkl} \langle u_l \theta \rangle \right] \tag{18}$$

$$\frac{D\langle \theta^2 \rangle}{Dt} - \frac{\partial}{\partial x_k}\left[lq\, S_\theta \frac{\partial \langle \theta^2 \rangle}{\partial x_k} \right] = -2\langle u_k \theta \rangle \frac{\partial \Theta}{\partial x_k} - \frac{2q}{\Lambda_2}\langle \theta^2 \rangle \tag{19}$$

where

$$P_s \equiv -\langle u_i u_j \rangle\, \partial U_i / \partial x_j \tag{20a}$$

is the shear production of turbulent energy,

$$P_b \equiv -\beta g_i \langle u_i \theta_v \rangle \tag{20b}$$

is the buoyant production, and

$$\varepsilon \equiv q^3/\Lambda_1 \tag{20c}$$

is the model dissipation.

(A mistake was made in the paper by *Mellor and Yamada* [1974]. The last term in their equation (21) and subsequent terms labeled $D_1 q^2$ in (52 *a*, *b*, *c*) and D_f in (55 *a*, *b*) and (56) should be purged, since they are of order $\mathbf{a}^2$. The mistake is embarrassing, since the original purpose of the ordering analysis was to eliminate terms.)

The Level 2½ Model

Subsequent to the *Mellor and Yamada* [1974] paper a further modification has been made to the level 3 model, the result of which is hereby labeled the level '2½' model.

The modification is to neglect the material derivative and diffusion terms in (15) or (19). This modification immediately removes the need to solve one differential equation but also is consistently applied to extensions where, say, water vapor (or salinity in the case of oceanic application) is added to the list of variables. Without the modification one would need to solve differential equations for temperature variance and water vapor variance and an equation for the cross correlation of water vapor and temperature. The situation quickly gets out of hand if more scalars are added to the list of computed variables. This change is not generally justified by our ordering analysis. However, a close reexamination of the ordering analysis indicates that the modification can be justified for all stable flows and slightly unstable flows; error is more likely as one approaches the free-convection limit. Nevertheless, our practical experience indicates that the modification should exert little effect on computed results.

We therefore replace (19) by

$$\langle \theta^2 \rangle = -\frac{\Lambda_2}{q}\langle u_k \theta \rangle \frac{\partial \Theta}{\partial x_k} \tag{21}$$

The Level 2 Model

This model neglects all material derivative and diffusion terms. Thus (16) is replaced by $P_s + P_b = \varepsilon$ and, further, consists of (17), (18) (which can be further simplified by the production-dissipation balance), and (21).

We note that a level 1 model was also identified by *Mellor and Yamada* [1974]. However, it fails to reproduce observational data (as in Figures 5*a* and 5*b*) and does not offer significant, compensatory mathematical simplification.

The Boundary Layer Approximation: Level 2½

For all subsequent versions of the model we will neglect the Coriolis term in the turbulence moment equation. This appears to be justified in boundary layers where lf/u_τ is small. (However, the issue probably should be investigated more thoroughly.) Note that if the Coriolis terms were retained, algebraic simplification of the type to be presented in this section does not appear possible; a large matrix inversion is required to obtain the fluxes for insertion into the mean equations of motion, (2) and (3).

Now, if one makes the boundary layer approximation, the vertical component of the momentum equation becomes hydrostatic, and in the other equations, all components of the tensor, $\partial U_j/\partial x_k$, may be neglected except for $\partial U/\partial z$ and

$\partial V/\partial z$. Then, if we set $g_i = (0, 0, -g)$, (2) and (3) simplify to

$$\rho \frac{D}{Dt} U + \frac{\partial}{\partial z} \rho\langle uw\rangle = -\partial P/\partial x + \rho f V \tag{22a}$$

$$\rho \frac{D}{Dt} V + \frac{\partial}{\partial z} \rho\langle vw\rangle = -\partial P/\partial y - \rho f U \tag{22b}$$

$$0 = -\partial P/\partial z - \rho g \tag{22c}$$

$$(D\Theta/Dt) + (\partial\langle w\theta\rangle/\partial z) = 0 \tag{23}$$

Although all model levels are simplified by virtue of the boundary layer approximation, levels $2\frac{1}{2}$ and 2 are most advantageously affected. Here we proceed with discussion of the level $2\frac{1}{2}$ model. Thus (16), after the boundary layer approximation, is

$$\frac{D}{Dt}\left(\frac{q^2}{2}\right) - \frac{\partial}{\partial z}\left[lqS_q \frac{\partial}{\partial z}\left(\frac{q^2}{2}\right)\right] = P_s + P_b - \varepsilon \tag{24}$$

where now

$$P_s = -\langle wu\rangle \frac{\partial U}{\partial z} - \langle wv\rangle \frac{\partial V}{\partial z} \tag{25a}$$

$$P_b = \beta g \langle w\theta\rangle_v \tag{25b}$$

$$\varepsilon = q^3/\Lambda_1 \tag{25c}$$

Equations (16), (17), and (18) may now be written as

$$\langle u^2\rangle = \frac{q^2}{3} + \frac{l_1}{q}\left[-4\langle wu\rangle \frac{\partial U}{\partial z} + 2\langle wv\rangle \frac{\partial V}{\partial z} - 2P_B\right]$$

$$\langle v^2\rangle = \frac{q^2}{3} + \frac{l_1}{q}\left[2\langle wu\rangle \frac{\partial U}{\partial z} - 4\langle wv\rangle \frac{\partial V}{\partial z} - 2P_B\right] \tag{26}$$

$$\langle w^2\rangle = \frac{q^2}{3} + \frac{l_1}{q}\left[2\langle wu\rangle \frac{\partial U}{\partial z} + 2\langle wv\rangle \frac{\partial V}{\partial z} + 4P_B\right]$$

$$\langle uv\rangle = \frac{3l_1}{q}\left[-\langle uw\rangle \frac{\partial V}{\partial z} - \langle vw\rangle \frac{\partial U}{\partial z}\right]$$

$$\langle wu\rangle = \frac{3l_1}{q}\left[-(\langle w^2\rangle - C_1 q^2) \frac{\partial U}{\partial z} + \beta g\langle u\theta_v\rangle\right] \tag{27}$$

$$\langle wv\rangle = \frac{3l_1}{q}\left[-(\langle w^2\rangle - C_1 q^2) \frac{\partial U}{\partial z} + \beta g\langle v\theta_v\rangle\right]$$

$$\langle u\theta\rangle = \frac{3l_2}{q}\left[-\langle uw\rangle \frac{\partial \Theta}{\partial z} - \langle w\theta\rangle \frac{\partial U}{\partial z}\right]$$

$$\langle v\theta\rangle = \frac{3l_2}{q}\left[-\langle vw\rangle \frac{\partial \Theta}{\partial z} - \langle w\theta\rangle \frac{\partial V}{\partial z}\right] \tag{28}$$

$$\langle w\theta\rangle = \frac{3l_2}{q}\left[-\langle w^2\rangle \frac{\partial \Theta}{\partial z} + \beta g\langle\theta\theta_v\rangle\right]$$

$$\langle\theta^2\rangle = -\frac{\Lambda_2}{q}\langle w\theta\rangle \frac{\partial \Theta}{\partial z} \tag{29}$$

If we further define

$$-\langle uw\rangle = K_M \partial U/\partial z \tag{30a}$$

$$-\langle vw\rangle = K_M \partial V/\partial z \tag{30b}$$

$$-\langle\theta w\rangle = K_H \partial\Theta/\partial z \tag{31}$$

$$K_M = lq\, S_M \tag{32a}$$

$$K_H = lq\, S_H \tag{32b}$$

and

$$G_M \equiv \frac{l^2}{q^2}\left[\left(\frac{\partial U}{\partial z}\right)^2 + \left(\frac{\partial V}{\partial z}\right)^2\right] \tag{33a}$$

$$G_H \equiv -\frac{l^2}{q^2}\beta g \frac{\partial \Theta_v}{\partial z} \tag{33b}$$

then (26), (27), (28), and (29) after considerable algebra reduce to

$$S_M[6A_1A_2G_M] + S_H[1 - 3A_2B_2G_H - 12A_1A_2G_H] = A_2 \tag{34}$$

$$S_M[1 + 6A_1{}^2G_M - 9A_1A_2G_H] - S_H[12A_1{}^2G_H + 9A_1A_2G_H] = A_1(1 - 3C_1) \tag{35}$$

which are readily solved (however, see discussion in section 6) for S_M and S_H as functions of G_M and G_H. From the definitions (25a)–(25c) and equations (30)–(33) it may be shown that

$$(P_s + P_b)/\varepsilon = B_1(S_MG_M + S_HG_H) \tag{36}$$

Looking ahead somewhat, contour plots of S_M, S_H, and $(P_s + P_b)/\varepsilon$ versus G_M and G_H are exhibited in Figure 3 after the empirical constants were determined.

Expressions for turbulence variances may be obtained. For example, the vertical velocity variance is given by

$$\langle w^2\rangle/q^2 = \tfrac{1}{3} - 2A_1S_MG_M + 4A_1S_HG_H \tag{37}$$

It is useful for later discussion to also write S_M and S_H as functions of G_H and $(P_s + P_b)/\varepsilon$. Thus using (36) to eliminate G_M from (34) and (35), we obtain

$$S_M[1 - (3A_2B_2 + 18A_1A_2)G_H] = A_2\left[1 - \frac{6A_1}{B_1}\frac{P_s + P_b}{\varepsilon}\right] \tag{38}$$

$$S_M[1 - 9A_1A_2G_H] - S_H[(18A_1{}^2 + 9A_1A_2)G_H] = A_1\left[1 - 3C_1 - \frac{6A_1}{B_1}\frac{P_s + P_b}{\varepsilon}\right] \tag{39}$$

The Boundary Layer Approximation: Level 2

A lower-order model is the level 2 model of *Mellor and Yamada* [1974], wherein the material derivative and diffusion terms in (16) and (19) are neglected so that production is balanced by dissipation. The level 2 model may be applied (to fairly good approximation it would appear) to an entire boundary layer but also applies rigorously in the limit as the surface is approached (and buoyancy effects vanish). Bound-

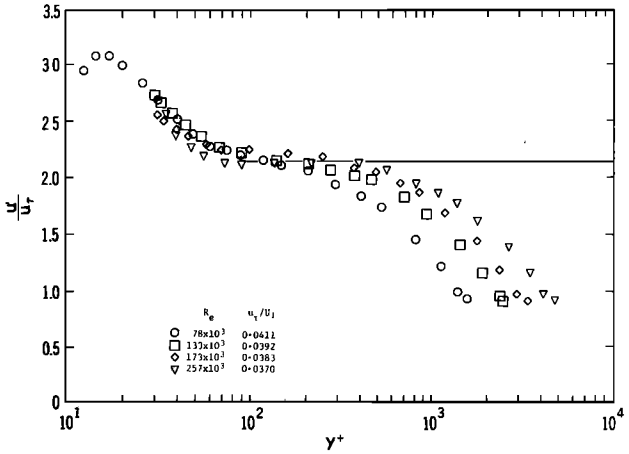

Fig. 1. Longitudinal turbulent intensity in a pipe as obtained by *Perry and Abell* [1975]. The horizontal line is the estimated outer asymptote of the inner function (law of the wall coordinates). The Reynolds number is based on the pipe diameter.

ary conditions for the higher-order models are obtained from the level 2 model.

If the boundary layer approximation is made and applied to (17), (18), and (21) after further simplification by virtue of the production-dissipation balance, then it is possible to obtain algebraic relations for S_M and S_H as functions of either flux Richardson number (see Figure 4)

$$R_f = -P_b/P_s \tag{40a}$$

or gradient Richardson number

$$R_i \equiv \frac{g\beta\,\partial\Theta/\partial z}{(\partial U/\partial z)^2 + (\partial V/\partial z)^2} = -\frac{G_H}{G_M} = \frac{S_M}{S_H} R_f \tag{40b}$$

The resulting relations are

$$S_H = 3A_2\,\frac{\gamma_1 - (\gamma_1 + \gamma_2)R_f}{1 - R_f} \tag{41a}$$

$$S_M = \frac{A_1}{A_2}\,\frac{B_1(\gamma_1 - C_1) - [B_1(\gamma_1 - C_1) + 6(A_1 + 3A_2)]R_f}{B_1\gamma_1 - [B_1(\gamma_1 + \gamma_2) - 3A_1]R_f}\,S_H \tag{41b}$$

where

$$\gamma_1 \equiv \tfrac{1}{3} - (2A_1/B_1) \tag{42a}$$

$$\gamma_2 \equiv (B_2/B_1) + (6A_1/B_1) \tag{42b}$$

As seen in (41*a*) and (41*b*), a critical Richardson number, where $S_M = S_H = 0$, is obtained when $R_f = \gamma_1/(\gamma_1 + \gamma_2)$. After evaluation of the constants A_1, B_1, and B_2 we will find that the critical Richardson number is 0.19.

Other quantities such as $\langle u^2\rangle/q^2$ and $\langle v^2\rangle/q^2$, may be obtained from (29)–(32) as functions of Richardson number.

We note that (41*a*) and (41*b*) may also be obtained from (33*b*), (38), and (39). First, set $(P_s + P_b)/\varepsilon = 1$ in (38) and (39). Then eliminate q^2 in (33*b*) using, again, $q^3 = \Lambda_1\varepsilon = \Lambda_1(P_s + P_b)$.

4. The Empirical Constants From Neutral Data

As stated previously, the constants A_1, B_1, A_2, B_2, and C_1 can be determined without resort to a trial and error process by appealing to data where turbulent energy production and dissipation are balanced. This occurs in the overlap (law of the wall) region near walls and in homogeneous shear flow data where diffusion is zero and where at some downstream point in the flow it happens that $\partial q^2/\partial x = 0$.

Mellor [1973] had previously determined that $(A_1, B_1, A_2, B_2, C_1) = (0.78, 15.0, 0.79, 8.0, 0.056)$. In this paper we have exerted more effort in collecting and interpreting data; hopefully, these results will also be useful to other modelers.

Interpretation of wall data to extract large Reynolds number results requires some care. We wish to correctly identify the outer (inviscid) asymptote of the 'inner,' viscous wall functions (law of the wall coordinates) which describe the various turbulent flow properties and which will match with the inner asymptotes of the 'outer' functions. It is the outer functions which our model is supposed to simulate. The large Reynolds number asymptotic behavior of turbulent wall flows has been discussed by *Yajnik* [1970] and *Mellor* [1972]. *Perry and Abell* [1975] have provided a nice experimental illustration of the matter, which we repeat here in Figure 1. It is seen that we need to determine a quantity like $u'/u_\tau \equiv \langle u^2\rangle^{1/2}/u_\tau$, where $y^+ \equiv yu/\nu \simeq 60$ and where $-\langle wu\rangle \simeq u_\tau^2 = \text{const}$. In general, data are not as well resolved in the near-wall regions as in Figure 1. Therefore there is likely error in interpretation. However, it is believed that this kind of error is considerably smaller than the variations among the different data sets related to measurement error.

The values for turbulent velocity variances are collected in Table 1, and those for turbulent thermal variances in Table 2. In Table 1, aside from Reynolds number and u_τ/U_0, the independent data may be thought to be u'/u_τ, v'/u_τ, and w'/u_τ; the remaining two quantities are derived. In Table 2, $-\langle w\theta\rangle/U_0\Delta\Theta$, $\theta'/\Delta\Theta$, and P_{rt} are independent, whereas the remaining two variables are derived.

We now simplify the model equations to the conditions governing the data in Tables 1 and 2, namely, that the flow is two dimensional, production equals dissipation, $-\langle uw\rangle \equiv u_\tau^2 = \text{const}$, $-\langle\theta w\rangle \equiv H = \text{const}$, and buoyancy effects are negligible. We next stipulate that

$$\partial U/\partial z = u_\tau/l \tag{43a}$$

which constitutes a partial definition of l; that is, any further prescription of $l(z)$ must be constrained so that $l = \kappa z$ near solid surfaces if the model is to reproduce the logarithmic law of the wall. Thus the 'master length scale' l is defined so that it is coincident with Prandtl's mixing length near solid surfaces, although it is here presumed to play a much broader role. A definition of turbulent Prandtl number $P_{rt} \equiv K_M/K_H$ and (30*a*), (31), (32*a*) and (35*b*) yield

$$\partial\Theta/\partial z = (H/u_\tau)(P_{rt}/l) \tag{43b}$$

Note that the turbulent Prandtl number will vary with stratification; in this discussion, only the neutral value is considered. Setting $l = \kappa z$, where $\kappa = 0.4$, and integrating (43*a*) and (43*b*) will yield laws of the wall equations for velocity and temperature, respectively.

Flows where production equals dissipation necessarily include flows near solid surfaces. Then $q^3/\Lambda_1 = -\langle uw\rangle\,\partial U/\partial z$, and from (43*a*) and (12),

$$q^3 = B_1 u_\tau^3 \tag{44a}$$

TABLE 1. Observed Values of Turbulent Velocity Variables Where Production Is Balanced by Dissipation

	$U_0X/\nu\ 10^{-4}$	u_τ/U_0	u'/u_τ	v'/u_τ	w'/u_τ	q/u_τ	$\langle uw\rangle/u'w'$
			Pipe				
Laufer [1954]	25.0	0.0346	2.2	1.70	1.00	2.95	0.45
Perry and Abell [1975]	12.8	0.0370	2.12		1.03		0.46
Bremhorst and Bullock [1973]	3.5	0.0398	1.9		1.26		0.42
			Channel				
Laufer [1950]	3.1	0.0377	1.88	1.19	1.03	2.45	0.52
Laufer [1950]	6.2	0.0367	1.74	1.14	1.03	2.32	0.55
Comte-Bellot [1965]			2.3	1.30	1.03	2.8	0.42
			Boundary Layer				
Klebanoff [1955]	7.4	0.0377	2.02	1.41	1.03	2.66	0.48
So and Mellor [1973]	2.0	0.042	1.70	1.18	1.00	2.30	0.58
Young et al. [1973]							
Flat surface	4.6	0.039	2.25		1.15		0.39
Wave surface	5.1	0.042	2.4		1.3		0.32
Wave surface	8.8	0.049	2.4		1.3		0.32
			Homogeneous Shear Flow				
Rose [1966]		0.0066	1.66	1.35	1.26	2.48	0.48
Champagne et al. [1970]		0.0105	1.70	1.29	1.20	2.45	0.49

Primes respresent rms values and $u_\tau^2 \equiv \langle uw\rangle$. U_0 is either the centerline velocity or the mainstream velocity. X represents pipe radius R, half channel width h, or boundary layer thickness δ.

Under the present constraints, equations (26) reduce to

$$\langle u^2\rangle = (1 - 2\gamma_1)q^2 \tag{44b}$$

$$\langle v^2\rangle = \langle w^2\rangle = \gamma_1 q^2 \tag{44c}$$

where γ_1 was previously defined in (42*a*) and

$$C_1 = \gamma_1 - \frac{1}{3A_1} B_1^{1/3} \tag{44d}$$

$$A_2 = \frac{A_1(\gamma_1 - C_1)}{\gamma_1 P_{rt}} \tag{44e}$$

$$B_2 = \frac{B_1^{1/3}}{P_{rt}} \frac{u_\tau^2\langle\theta^2\rangle}{H^2} \tag{44f}$$

We must choose values of B_1, γ_1, P_{rt}, and B_2 from Tables 1 and 2. It is not a simple choice, and perhaps the principal value of the tables is to show that some uncertainty exists; if we bias our choice toward one set of data, that set will be predicted well, but another set may not be. For example, there is an obvious difference between the wall data and the homogeneous shear flow data.

The first choices we have made are $B_1 = 16.6$ and $\gamma_1 = 0.222$. From (42*a*) and (44*d*) we obtain $A_1 = 0.92$ and $C_1 = 0.08$. From (44*a*)–(44*c*) this yields $q/u_\tau = 2.55$, $u'/u_\tau = 1.9$, and $v'/u_\tau = w'/u_\tau = 1.2$. The fact that v' and w' are equal is not supported by the data, and as discussed earlier, the model could be complicated to permit $v' \neq w'$. The choice of additional terms is not clear, however, and the further choice of the additional constants they would introduce would be less clear.

The choice of turbulent Prandtl number is quite ambiguous from Table 2. This quantity has been measured by others besides those listed in Table 2. A 1961 survey [*Kestin and Richardson*, 1961] infers that near a smooth wall, $0.74 < P_{rt} < 0.92$. *Gowen and Smith* [1968] obtain $0.8 < P_{rt} < 1.0$ for smooth pipes and $1.0 < P_{rt} < 1.2$ for rough pipes at a radius Reynolds number of 20,000. (For large enough Reynolds number, P_{rt} should not depend on roughness.) Atmospheric boundary layer data, to be discussed below, indicate $P_{rt} = 0.74$ in the neutral case. Here we choose $P_{rt} = 0.80$, so that (44*e*) yields $A_2 = 0.74$. Finally, we choose $B_2 = 10.1$. Using (44*f*), this yields $u_\tau^2\langle\theta^2\rangle/\langle w\theta\rangle^2 = 3.1$, which may be compared with the corresponding data in Table 2. Perhaps it is better to consider the correlations $(-\langle uw\rangle)/(u'w')$ and $(-\langle w\theta\rangle)/(w'\theta')$ which can be calculated from the above constants and equations. We obtain 0.44 and 0.42 for com-

TABLE 2. Observed Values of Turbulent Thermal Variables Where Production is Balanced by Dissipation

	$U_0X/\nu\ 10^{-4}$	$\langle w\theta\rangle/U_0\Delta\Theta$	$\theta'/\Delta\Theta$	P_{rt}	$\langle w\theta\rangle/w'\theta'$	$u_\tau^2\langle\theta^2\rangle/\langle w\theta\rangle^2$
			Pipe			
Bremhost and Bullock [1973]	3.5	0.0020	0.102		0.41	3.0
			Boundary Layer			
Young et al. [1973]						
Flat surface	4.6	0.0015	0.075	0.95	0.46	3.8
Wave surface	5.1	0.0032	0.12	0.55	0.48	2.48
Wave surface	8.8	0.0035	0.11	0.55	0.50	2.37

Primes represent rms values. $\Delta\Theta$ is either the centerline or the mainstream temperature minus the wall temperature. X represents either pipe radius R or boundary layer thickness δ.

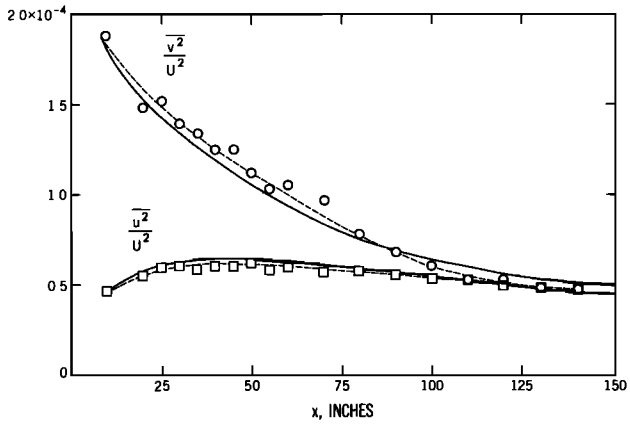

Fig. 2*a*. Data by *Uberoi* [1957] for a homogeneous anisotropic flow. The dashed lines are faired through the data points, whereas the solid lines are model generated.

parison with those data. It should also be noted that similarity considerations yield $B_2/B_1 = 2/3$ for decaying, homogeneous temperature and velocity fields [*Hinze*, 1975, p. 300], which apparently agrees with the measurements of *Gibson and Schwartz* [1965]. However, these measurements cover a rather short decay history.

Summarizing, we find now that

$$(A_1, B_1, A_2, B_2, C_1) = (0.92, 16.6, 0.74, 10.1, 0.08) \qquad (45)$$

which differ just a bit from values cited previously which were evaluated with less information.

Uberoi's Experiment

All of the results above were obtained independent of a prescription for $l(x)$. Proceeding in the same vein, we turn to experiments performed by *Uberoi* [1956, 1957] whereby near-homogeneous, anisotropic turbulence was created in a wind tunnel by the combination of a turbulence-producing grid followed by a tunnel cross-sectional area contraction resulting in an initial condition where $\langle w^2 \rangle = \langle v^2 \rangle > \langle u^2 \rangle$; x and $\langle u^2 \rangle$ are the coordinate and turbulence energy component in the tunnel flow direction. The governing equation for $\langle u^2 \rangle$, $\langle v^2 \rangle$, $\langle w^2 \rangle$ is

$$U \frac{\partial \langle u_\alpha{}^2 \rangle / 2}{\partial x} = \left\langle p \frac{\partial u_\alpha}{\partial x_\alpha} \right\rangle - \frac{\varepsilon}{3} \qquad \alpha = x, y, z$$

We use Greek subscripts to denote suspension of the summation convention. Note that we assume that the dissipation is isotropic; but that is the only assumption necessary to reduce the data so that it is very nearly a direct test of Rotta's hypothesis. Measurements of $\langle u^2 \rangle(x)$ and $\langle v^2 \rangle = \langle w^2 \rangle(x)$ from *Uberoi* [1957] are plotted in Figure 2*a*. Values of $\langle u^2 \rangle$ and $\langle v^2 \rangle = \langle w^2 \rangle$ are obtained at each data point location but from the smoothed curve passed through the data by Uberoi (dashed line). From these data and the above equation it is possible to obtain values of $\langle p\, \partial u/\partial x \rangle$, $\langle p\, \partial v/\partial x \rangle$, and ε as functions of x. Thus in Figure 2*a* we plot the ratios $\langle p\, \partial u/\partial x \rangle/(\varepsilon/3)$ and $\langle p\, \partial v/\partial x \rangle/(\varepsilon/3)$ (to eliminate length scales) as a function of $(u^2 - q^2/3)/(q^2/3)$ and $(v^2 - q^2/3)/(q^2/3)$, respectively, to compare with

$$\left\langle p \frac{\partial u_\alpha}{\partial x_\alpha} \right\rangle \Big/ (\varepsilon/3) = -\frac{B_2}{6A_1} \frac{\langle u_\alpha{}^2 \rangle - q^2/3}{q^2/3} \qquad (46)$$

which may be obtained from (4) and (5). The results are presented in Figure 2*b* as circles and squares along with the straight-line plot of (46) where, using the constants previously obtained in (45), we determine that $B_1/(6A_1) = 3.00$.

We now note that the solid line in Figure 2*a* is a model prediction which embodies (46) but also requires a length scale prescription. While in this section we do not yet wish to emphasize the latter, the solid curve is a useful reference to emphasize that small error in data as plotted in Figure 2*b* would result in apparent large error in Figure 2*a*, particularly near the origin of Figure 2*b*; this region of small anisotropy is where we would most likely expect Rotta's hypothesis to be valid.

On the other hand, the reader will observe data (crosses) for larger anisotropy which departs significantly from Rotta' hypothesis. The departures seem overly abrupt. Nevertheless, the abscissa values, −1.0 and 0.5, in Figure 2*a* represent the limits for two-dimensional, axisymmetric turbulence where $\langle v^2 \rangle = 0$ and $\langle u^2 \rangle = \langle w^2 \rangle$. At these limits one should anticipate that Rotta's hypothesis might fail. In fact, it appears from Figure 2*a* that it fails when the smallest component is $\langle v^2 \rangle/\langle q^2 \rangle \simeq 0.12$.

The grid Reynolds number for the Uberoi experiments was 12,000 and therefore not very large. Corroborative experiments are not available. Nevertheless, the principal results support Rotta's hypothesis, support the choice of empirical constants (obtained from entirely independent data where production and dissipation balance), and place a limit on the range of applicability of Rotta's hypothesis.

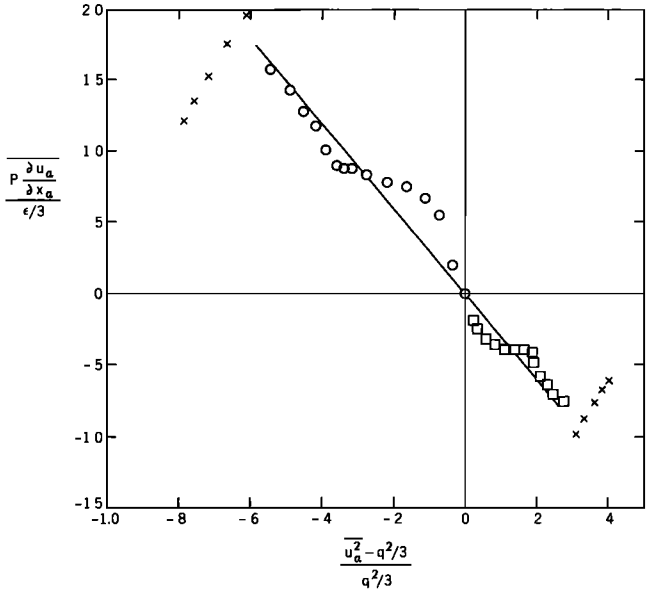

Fig. 2*b*. The solid straight line is obtained from (4) and (20*c*) and the slope is $-B_1/(6A_1) = 3.00$ as obtained from (45). The open circles and squares are from *Uberoi* [1957], whereas the crosses are from *Uberoi* [1956].

5. Stabilization by Density Stratification and Flow Curvature

The model has not yet been described completely, but enough has been determined to demonstrate the surprising capability of the model to predict the stabilization of turbulent fields by density stratification and curvature. The data obtained by *So and Mellor* [1973] were a clear demonstration

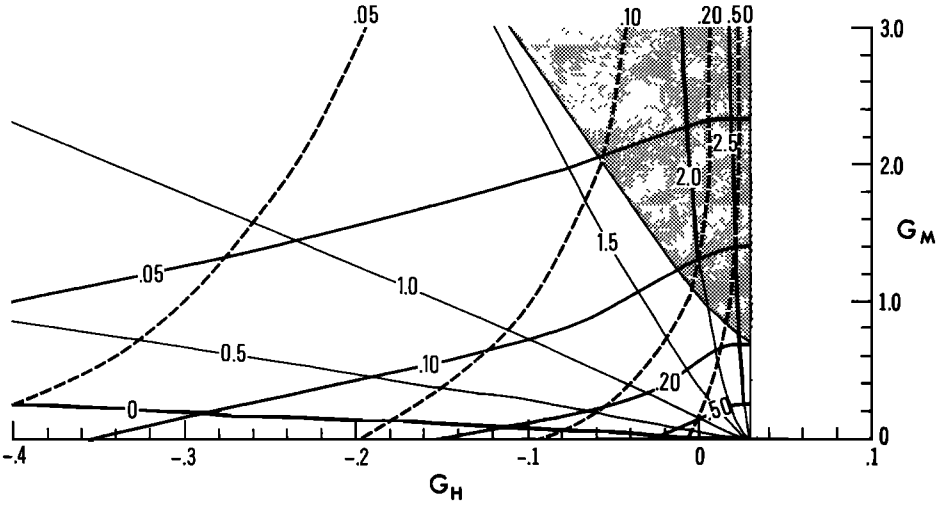

Fig. 3. The stability functions $S_M(G_H, G_M)$ and $S_H(G_H, G_M)$. The heavy solid lines are contours of S_M, whereas the dashed lines are contours of S_H. The lighter solid lines are contours of $(P_s + P_b)/\varepsilon$. One could also draw lines of constant $R_i = G_H/G_M$, which are radial lines on this diagram. The shaded portion is where $\langle w^2\rangle/q^2 \lesssim 0.12$.

of the fact that stabilizing curvature could literally extinguish turbulence. The effect of curvature as predicted by the model has been described by *So* [1975] and *Mellor* [1975] and was important corroboration that the model could predictively extend far beyond the neutral data on which it is based. However, this paper is meant to emphasize geophysical fluid problems, for which we will shortly turn to the near-surface, atmospheric boundary layer data of *Businger et al.* [1971].

Using the constants in (45), the level $2\frac{1}{2}$ functions, $S_M(G_M, G_H)$ and $S_H(G_M, G_H)$, are plotted in Figure 3 from (34) and (35). Contours of $(P_s + P_b)/\varepsilon$ are also plotted. As the limit $G_H = 0.0338$ is approached, we find that $S_H \to \infty$. In principle this means that gradients such as $\partial\Theta/\partial z$ will be mixed out with an indefinitely large value of K_H such that G_H cannot exceed the limiting value. On this graph one can identify probable limits to the model's validity. The upper right portion of Figure 3 is a region where $\langle w^2\rangle/q^2 < 0.12$, representing (approximately) a region where Rotta's hypothesis is probably invalid. *Dickey and Mellor* [1980] have found experimentally that for stratified homogeneous, decaying turbulence the point $G_M = 0$, $G_H \simeq -0.4$ is reached where the initial turbulence is converted into an ensemble of internal waves which decay very slowly (or, probably, not at all in the limit of large Reynolds number). We therefore know that (5) is no longer valid, and this is probably true for the other modeling assumptions. This may not be a serious deficiency, since the model should produce very low turbulence levels and little mixing for the aforementioned values of G_M and G_H.

Figure 4 (corresponding to the cross section given by $(P_b + P_s)/\varepsilon = 1$ of Figure 3) is a plot of the level 2 functions $S_M(R_f)$ and $S_H(R_f)$ from (41) and (42). A critical Richardson number $R_f \simeq R_i = 0.19$ is obtained beyond which $S_M = S_H = 0$.

For the purpose of direct comparison of data with model prediction we apply the level 2 model where all material derivative and diffusion terms in the turbulent moment equations have been neglected. This should be a valid simplification near surfaces, at least for neutral and stable flows. For near-surface flows we also assume $l = kz$. The data are cast in Monin-Obukhov similarity form, $\phi_M(\zeta)$, $\phi_H(\zeta)$, where

$$\phi_M \equiv \frac{\kappa z}{u_\tau}\frac{\partial U}{\partial z} = [B_1(1 - R_f)S_M{}^3]^{-1/4} \tag{47a}$$

$$\phi_H \equiv \frac{\kappa z u_\tau}{H}\frac{\partial \Theta}{\partial z} = [B_1(1 - R_f)S_H{}^4/S_M]^{-1/4} \tag{47b}$$

$$\zeta \equiv \frac{z}{u_\tau{}^3/(\kappa g \beta H)} = \phi_M R_f \tag{47c}$$

and where $u_\tau{}^2 = (\langle uw\rangle^2 + \langle vw\rangle^2)^{1/2}$ and $H = -\langle w\theta\rangle$ near the surface.

Figures 5*a* and 5*b* compare the model results with the data of *Businger et al.* [1971]. Note that the point $R_f = R_{fcr} = 0.19$ in Figure 4 is mapped into the straight lines in Figures 5*a* and 5*b* as $\zeta \to \infty$. Note also that the prediction of R_{fcr} does not depend on $l(z)$.

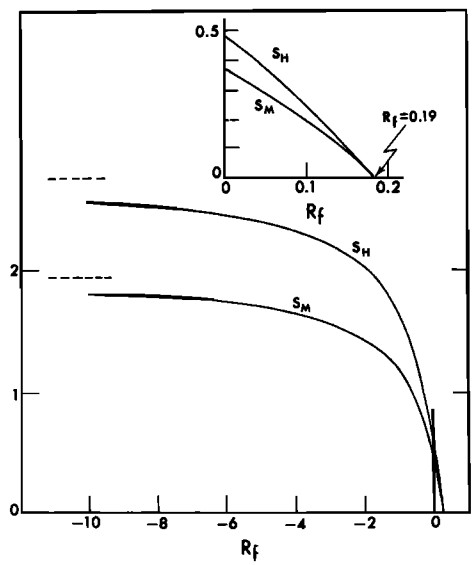

Fig. 4. The stability functions S_M and S_H as a function of flux Richardson number corresponding to the condition $(P_s + P_b)/\varepsilon = 1$ of Figure 3.

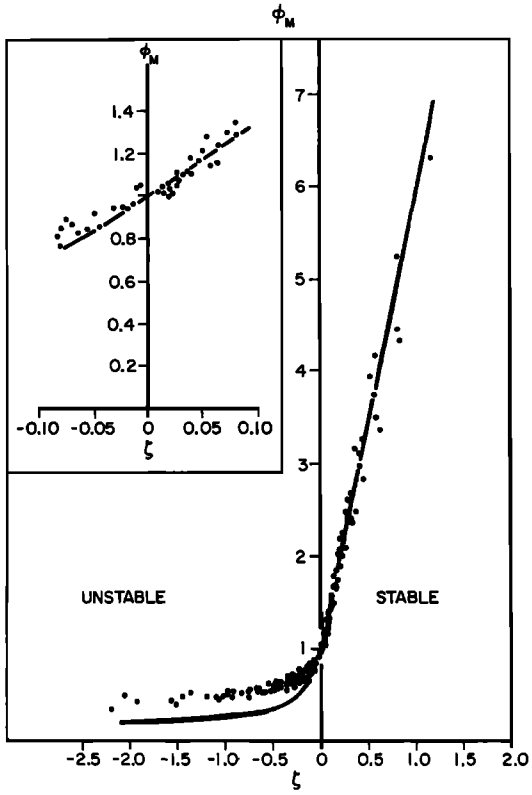

Fig. 5a. Comparison of the velocity profile data of *Businger et al.* [1971] with predicted values (solid curve). Insert is detail near $\zeta = 0$.

The fact that the basic model has the predictive capability of extrapolating neutral data into stratified regimes was probably the most important finding [*Mellor*, 1973] in the development of the model.

Lewellen and Teske [1973] have also shown a favorable comparison of their model with these data. They included the diffusion term and did get better agreement than we did for ϕ_M in the unstable region where diffusion is liable to be important. However, they had to insert a specific Richardson number parameterization into their model to obtain the correct critical Richardson number. *Gambo* [1978] also obtained improvement in ϕ_M in the unstable region by including buoyancy terms in (4) in a manner described at the end of section 2; however, agreement with the stable data for both ϕ_M and ϕ_H was not as good as that shown here.

It should be noted that the Businger data were also evaluated to yield a von Karman constant κ of 0.35, somewhat less than the more commonly accepted value of 0.40. *Wieringa* [1980] discusses the issue, reevaluates the data taking into account tower interference, and argues in favor of the value 0.40. The later value is used throughout this paper.

6. The Turbulent Length Scale Equation

We have postponed consideration of the equation for the master length scale l so that the other elements of the model were first justified on the basis of neutral data and a direct test of the model's predictive power, that is, the prediction of turbulent stabilization in a density-stratified flow. The factor S_q in (24) must also now be determined.

Following *Rotta* [1951], we use the integral of the two-point correlation function to supply an equation for the master length scale. The closure assumptions are complicated, and we consider the result less convincing than the previous assumptions and more likely to be amended in the future. The version we have used for some time (see *Mellor and Herring* [1973] for a general discussion) is

$$\frac{D}{Dt}(q^2 l) - \frac{\partial}{\partial z}\left[qlS_l \frac{\partial}{\partial z}(q^2 l) \right] = lE_1[P_s + P_b] - \frac{q^3}{B_1}\left\{1 + E_2\left(\frac{l}{kL}\right)^2\right\} \tag{48}$$

For neutral, homogeneous, decaying grid turbulence where l is much smaller than L, (48) along with (26) predicts the initial period decay law, $q^2 \propto t^{-1}$. S_l, E_1, and E_2 are empirical constants to be determined. P_b might be preceded by another constant if data can be found to unambiguously support a value other than unity.

L is supposed to be a measure of the distance away from the wall as is specified according to

$$L^{-1}(\mathbf{r}) = \frac{1}{2\pi} \iint \frac{dA(\mathbf{r}_0)}{[r - r_0]^3} \tag{49}$$

which is similar to ideas offered by *Shir* [1973] and *Launder et al.* [1975]. Here $\mathbf{r}$ is any point in the fluid domain bounded by solid wall at $\mathbf{r}_0$; $dA(\mathbf{r}_0)$ is an elemental wall area. For a boundary layer flow near an infinite plane wall, $L = z$; for channel flow, $L^{-1} = z^{-1} + (2h - z)^{-1}$, where $2h$ is the distance separating the channel walls. It can, by the way, be shown that a third term on the right of (48), here represented

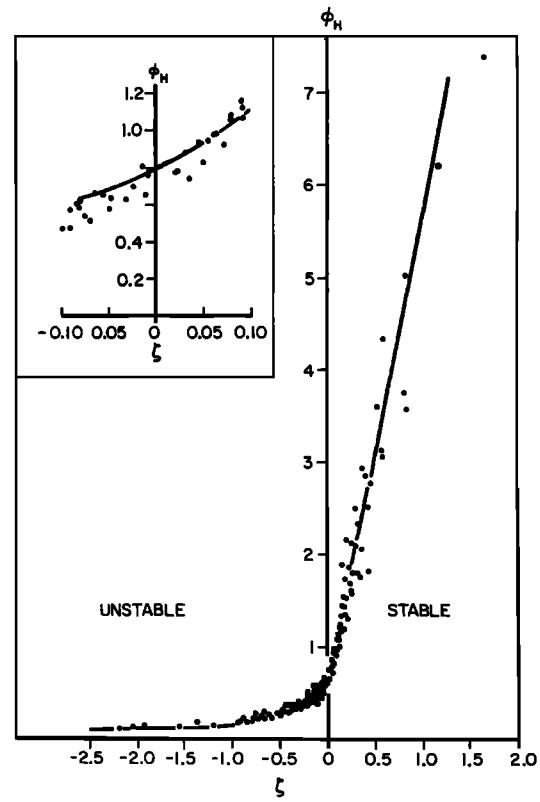

Fig. 5b. Comparison of the temperature profile data of *Businger et al.* [1971] with predicted values (solid curve). Insert is detail near $\zeta = 0$.

by $(q^3/B_1)E_2\ (l/\kappa L)^2$, is absolutely necessary, but the one chosen here is one of several alternatives [*Ng and Spalding*, 1972; *Wolfstein*, 1970; *Mellor and Herring*, 1973; *Lewellen et al.*, 1976; *Rotta*, 1973]. All one can say in the present case is that, as we will see, it works well.

While one cannot assert great confidence in (48), we prefer it rather than the differential equation for dissipation [*Daly and Harlow*, 1970; *Hanjalic and Launder*, 1972; *Lumley and Khajeh-Nouri*, 1974]. The dissipation transport equation is an equation for the curvature of the two-point, velocity correlation function as the separation distance approaches zero (for large Reynolds number, the transport terms, per se, are negligible, as shown by *Tennekes and Lumley* [1972]). Alternatively, it is an equation for the integral of the spectral density function after multiplication by the square of the wave number, thus weighting the integral so that large wave number and small-scale turbulence are emphasized. Thus it seems fundamentally wrong to us to use an equation which describes the small-scale turbulence to determine the required turbulent macroscale. Operationally, however, after some terms are modeled, the dissipation transport equation is a special case of a more general length scale equation [*Mellor and Herring*, 1973; *Lewellen et al.*, 1976].

In subsequent discussions we will mention some calculations using the level 2 model and an algebraic expression of the form

$$l = l_0 \frac{kz}{kz + l_0} \qquad l_0 \equiv \alpha \frac{\int_0^\infty |z| q\, da}{\int_0^\infty q\, dz} \tag{50}$$

in place of (48). For boundary layers this works well, but it is limited to boundary layers, and the empirical constant α would depend on the type of layer, for example, a boundary layer as in Figure 7 or an Ekman layer. Some studies actually simplify (50) further so that $l = l_0$. This will not produce a logarithmic velocity behavior near surfaces. However, for the case of an ocean surface mixed layer the additional simplification does not seem to impact mixed layer deepening or temperature.

Boundary Conditions

We have postponed stipulation of boundary conditions until this time when the complete set of model differential equations are available.

For the mean velocity and temperature boundary condition near a surface at $z = z_0$, one either specifies stress and heat flux,

$$-\langle wu_i\rangle(x, y, z_0) \equiv \tau_{0i} \sim (qlS_M\, \partial U_i/\partial z) \qquad z \to z_0 \tag{51}$$

$$-\langle w\theta\rangle(x, y, z_0) \equiv H \sim (qlS_H\, \partial\Theta/\partial z) \qquad z \to z_0 \tag{52}$$

or, near solid surfaces at rest, the numerical solution is matched to

$$U_i(x, y, z) \sim \frac{\tau_{0i}}{\kappa u_\tau} \ln\left(\frac{z - z_0}{z_{MS}}\right) \qquad z \to z_0 \tag{53a}$$

$$\Theta(x, y, z) - \Theta(x, y, z_0) \sim \frac{HP_{rt}}{\kappa u_\tau} \ln\left(\frac{z - z_0}{z_{HS}}\right) \qquad z \to z_0 \tag{53b}$$

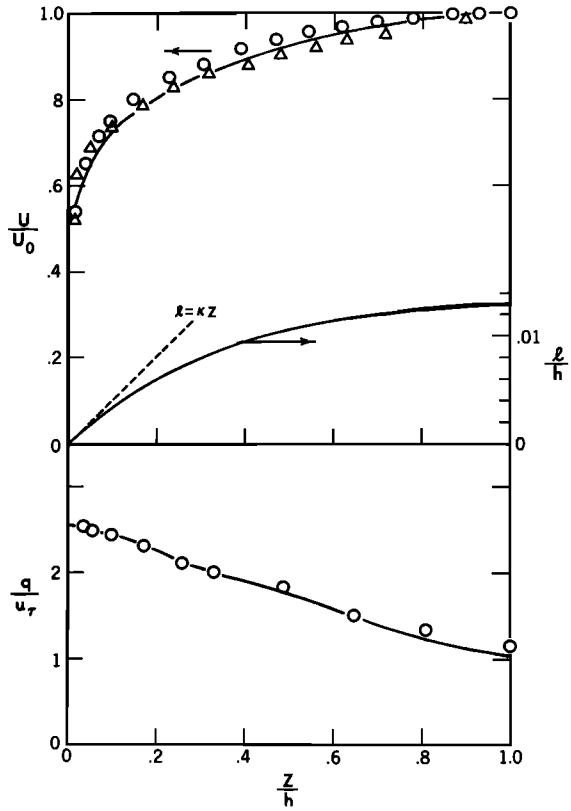

Fig. 6. Channel flow. Comparison of predicted mean velocity and turbulent intensity (solid lines) with data by *Lauffer* [1950] and by Hanjalic as recorded by *Launder et al.* [1975]. The circles are Lauffer's data.

where $u_\tau^2 \equiv (\tau_{0i}^2)^{1/2}$, $i = x, y$, and z_{MS} and z_{HS} are the roughness parameters; for smooth surfaces, $z_{MS}u_\tau/\nu = \exp(-4.9\kappa)$, whereas z_{HS}/z_{MS} is a function of Prandtl number.

Asymptotically close to surfaces, all equations for the turbulence variances reduce to the level 2 algebraic equations. Furthermore, the buoyancy production terms vanish. Thus for the level 2½ model we have from (44*a*)

$$q^2(x, y, z_0) = B_1^{2/3} u_\tau^2 \tag{54}$$

to which we add

$$q^2 l(x, y, z_0) = 0 \tag{55}$$

on solid surfaces. For free-stream conditions the mean velocity and temperature are specified. If the free-stream turbulence is known, that is specified. Otherwise, a very small value is used. Solutions are quite insensitive to free-stream values of $q^2 l$.

For the level 4 and level 3 models, additional boundary conditions are obtained from (26)–(29) after replacing $P_B = 0$, $\partial U/\partial z = -\langle uw\rangle/(\kappa u_\tau z)$, and $\partial V/\partial z = -\langle vw\rangle/(\kappa u_\tau z)$; some results are given in (44*b*) and (44*c*).

Neutral Channel Flow and Boundary Layer Flow

Calculations were made for channel flow and a constant pressure boundary layer to assess S_q, S_l and E_1, E_2. It became apparent that one should set $S_l = S_q$; otherwise the behavior of l in the center of the channel or at the edge of the boundary layer was unrealistic. To insure that $l \sim \kappa z$ as $z \to 0$, it may be shown that $E_2 = \kappa^2 B_1 S_l + E_1 - 1$. The values of

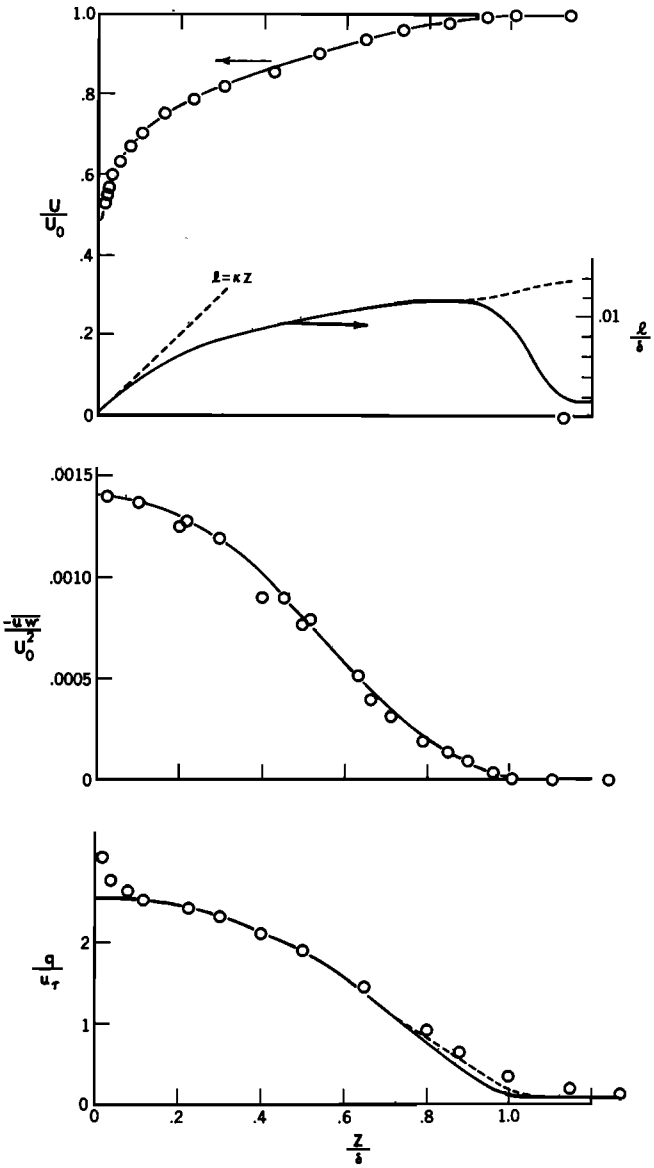

Fig. 7. Boundary layer. Comparison of the predicted mean velocity and turbulent intensity with data by *Klebanoff* [1955].

S_q and E_1 are then chosen to optimize agreement between model results and data at the center and outer edge of the channel and boundary layer, respectively. An agreeable result was that the values $S_q = 0.2$ and $E_1 = 1.8$ were optimum for both flows. Thus we obtain $(S_q, S_l, E_1, E_2) = (0.2, 0.2, 1.8, 1.33)$ and the predictions shown in Figures 6 and 7. In both cases there is near-perfect agreement with measured values of $-\langle uw\rangle(z)$ and $q(z)$. For the channel flow case the observed and calculated Reynolds stress distributions are linear and are not shown.

The outer free-stream turbulence level for the boundary layer flow has been set at $q/u_\tau = 0.07$ as estimated from *Klebanoff* [1955], but this may be a bit low. Two boundary conditions for q^2l have been specified and correspond to the calculated solid and dashed lines in Figure 7.

The separate components u', v', and w' are not shown, since they do not enter into the determination of E_1. Agreement with data is quite good in this respect except that we predict $v' = w'$ as discussed earlier. Away from walls this is in agreement with the data, but near walls there is some disagreement in accordance with Table 1.

In unpublished work we have also calculated circular duct flow after (26), (47), and (48) are cast in cylindrical coordinate form, and these calculations compared favorably with the duct flow data of *Laufer* [1954].

This is perhaps an appropriate place to record the fact that we have had occasional difficulty with the level $2\frac{1}{2}$ model; for some model simulations a discontinuity in velocity could develop and persist. We will not detail the nature of the problem here except to note that its occurrence depends on the specifics of finite differencing. Thus it occurs when Reynolds stresses and mean velocities are staggered with respect to each other but not when these variables are located at the same grid points. It further occurs when $(P_s + P_b)/\varepsilon$ attains large values (unrealistically greater than 2) as, for example, when wind stress is impulsively applied to an ocean surface initially at rest with initially zero layer thickness. A modified level $2\frac{1}{2}$ model [*Worthem and Mellor*, 1980] obviated the problem but required a complicated iteration. More recently, however, we have reverted to the original scheme (equations (26)–(29)) after we learned that the problem can be avoided by constraining the domain of dependence of the $S_M(G_M, G_H)$ functions so as to exclude the regions where $\langle w^2\rangle/q^2 \leq 0.12$ (the shaded region in Figure 3) and where, according to the discussion in section 4, Uberoi's data present reason to believe that Rotta's assumption fails. Of course, one might accordingly revise Rotta's hypothesis, but that step might better await further corroborative data. It would also complicate the model and, it is believed, unnecessarily so for most practical problems.

The constraint we use on (34) and (35) is $G_H \leq 0.033$ and $G_M \leq 0.825 - 25.0\, G_H$.

7. Further Geophysical Applications

The models as described thus far, mainly in the context of one-dimensional simulations, have now matured sufficiently so that these form the basis for other one-dimensional investigations to compare model predictions with laboratory flows and to generate new information on boundary layer responses. The closure models have also been incorporated into larger, three-dimensional atmospheric and oceanographic numerical models. The following discussion will highlight some of these applications.

Free Convection

With no alteration in the model, level $2\frac{1}{2}$ calculations are performed to compare with the free-convection experiment of *Willis and Deardorff* [1974] wherein a heat flux was imposed at the bottom surface of a tank of water after a linear temperature gradient had been established in the tank. Since there is no shear production, the Richardson number changes abruptly from $+\infty$ to $-\infty$ at $z = z_i$, the inversion height.

The calculated temperature and heat flux very nearly overlie the data in Figure 8 and have not been plotted. A possible exception is that the small, negative flux overshoot near the inversion height, $z = z_i$, is underestimated by a factor of 3 or 4. Note that the experimental heat flux was determined by integrating the temperature tendency and might be subject to error.

The predictions of $\langle w^2\rangle$ and $\langle\theta^2\rangle$ in Figures 9 and 10 agree well with the data, whereas $\langle u^2\rangle$ does not. Furthermore, free-

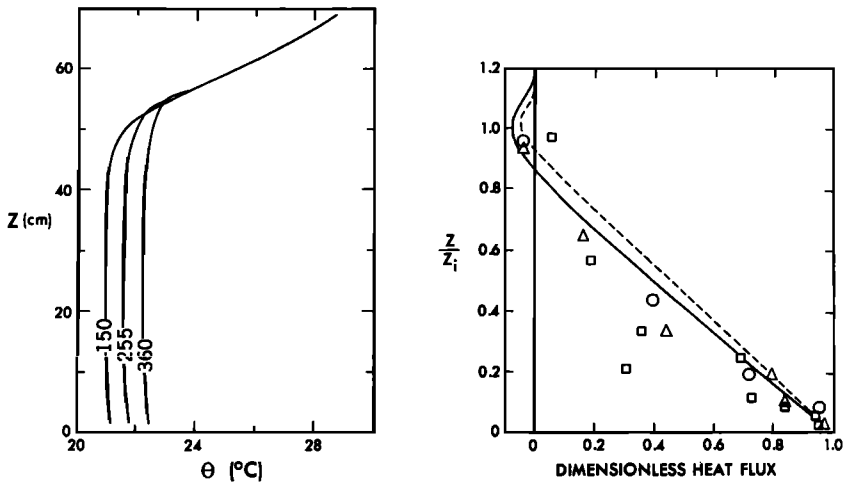

Fig. 8. Mean temperature and heat flux profiles from the laboratory experiment of *Willis and Deardorff* [1974]. Calculated profiles were nearly coincident with these data. Open data points are atmospheric aircraft measurements in conditions thought to be similar to those of the laboratory experiment.

convection scaling 'laws' where $\langle w^2 \rangle \propto (g\beta Hz)^{2/3}$ and $\langle \theta^2 \rangle \propto H^2(g\beta Hz)^{-2/3}$ as $z \to 0$ are seen to prevail for these quantities but not for $\langle u^2 \rangle$ as $z \to 0$. In other words, both the scaling laws and the model fail to represent $\langle u^2 \rangle$ well near the surface. As discussed by *Sun and Ogura* [1980], a rationalization for this finding is that $\langle u^2 \rangle$ is dependent on both z and z_1, the overall height of the boundary layer.

It should be noted that the sharp minimum in $\langle \theta^2 \rangle$ near $z = 0.7z_i$ would undoubtedly be modified by a level 3 model calculation which includes diffusion of $\langle \theta^2 \rangle$.

Readers might wish to compare the results of Figures 8, 9, and 10 with similar results obtained by *Lewellen et al.* [1976], *Zeman and Lumley* [1976], *Sun and Ogura* [1980], and *Andre et al.* [1976*b*]. The latter solved the aforementioned difficulty with the $\langle u^2 \rangle$ problem by setting their length scale to a constant proportion to z_i and by matching their lower boundary conditions to the data.

It should be noted that *Willis and Deardorff* [1974] also obtained data for $\langle wq^2 \rangle/2$. If $\langle pw \rangle$ were zero, one could compare those data with the diffusion represented by $ql\,S_q{}^2\,(q^2/2)/\partial z$ in (24) (even though we formally neglected pressure diffusion, it must, as discussed in section 2, be considered a part of the diffusion term (24) if observations indicate that $pw \neq 0$), in which case the model appears to underestimate the measured $\langle wq^2 \rangle$.

The observational determination of net turbulent diffusion importantly depends on the measured behavior of the dissipation. Since the buoyancy production must decrease linearly, or nearly so, with height, it may be inferred that net diffusion is small if dissipation behaves similarly.

Lenschow [1970] and *Kukharets and Tsvang* [1977] observed dissipation rate profiles that were almost uniform with height in the middle regions of the convective mixed layer. Also, the explicit turbulent simulation model of *Deardorff* [1974] produced pressure diffusion that was small and velocity diffusion that was comparable to dissipation. On the other hand, nearly linear dissipation rate profiles were observed by *Yokoyama et al.* [1977] over land and by *Pennel and LeMone* [1974] over the tropical ocean.

Also, *Caughey and Wyngaard* [1979] have, in an atmospheric convection layer, measured buoyancy production, dissipation, and turbulent velocity diffusion and by difference determined that pressure diffusion is of opposite sign to velocity diffusion and, in fact, they tend to cancel.

When the observational record is clarified, the model might be suitably modified.

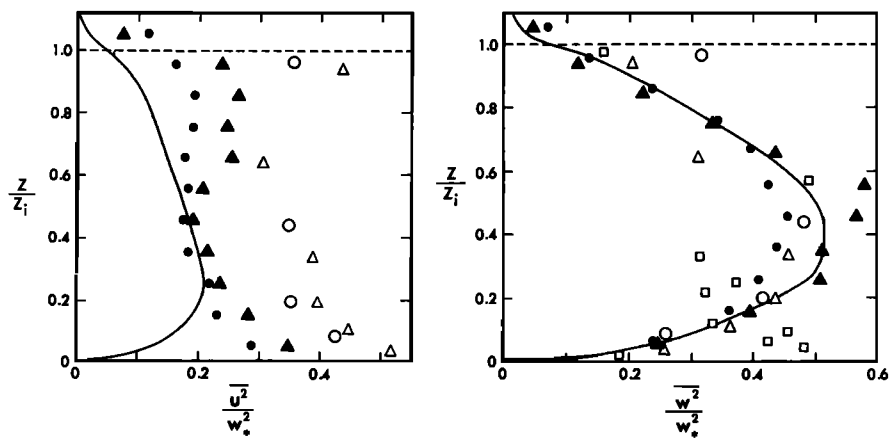

Fig. 9. Horizontal and vertical turbulent energy components (solid symbols) by *Willis and Deardorff* [1974]. Open data symbols are aircraft measurements, solid lines are calculated, and $w_* \equiv (g\beta Hz_i)^{1/3}$.

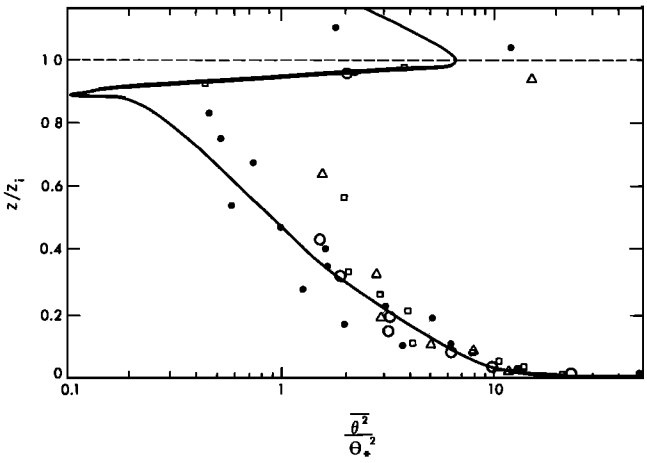

Fig. 10. Temperature variance (solid symbols) by *Willis and Deardorff* [1974]. Open data symbols are aircraft measurements, solid lines are calculated, and $\theta_* \equiv H/w_*$.

It is reasonable to expect that S_q in (26) is Richardson number dependent as are, analogously, S_M and S_H. We have, in fact, computed the *Willis and Deardorff* [1974] experiment with S_q = const = 0.2 and with $S_q \propto S_M$ (where the constant of proportionality is adjusted so that $S_q = 0.2$ in the neutral flow limit). The difference in the calculated results were not large.

Forced Convection

The experiment whereby a shear stress was impulsively applied to the top surface of stable, salinity-stratified water, thereby mixing the top layer, has been performed by *Kato and Phillips* [1969]. Qualitatively, the mixing process is inhibited by the stratification such that an abrupt density change occurs across the interface separating strongly turbulent and quiescent fluid. Using the simpler, level 2 version of the model (an algebraic length scale recipe and neglect of the turbulent kinetic energy tendency and diffusion terms), *Mellor and Durbin* [1975] predicted these data quite well, and we expect that prediction will prevail when this latest version of the model is applied. Other examples of mixed layer dynamics are explored and a favorable comparison with ocean observations in the North Pacific is included in the paper by Mellor and Durbin. The level $2\frac{1}{2}$ model has also been favorably compared to the two-level experiment of *Kantha et al.* [1977] by *Mellor and Strub* [1980].

8. Atmospheric and Oceanographic Simulations

The Wangara Data Set

The present model has been compared with atmospheric boundary layer data of *Clarke et al.* [1971], which are called the 'Wangara data.' The temperature variables in the previous equations must now be interpreted as virtual potential temperature.

Comparison of simulations and observations by *Yamada and Mellor* [1975] are shown in Figures 11–13. The calcula-

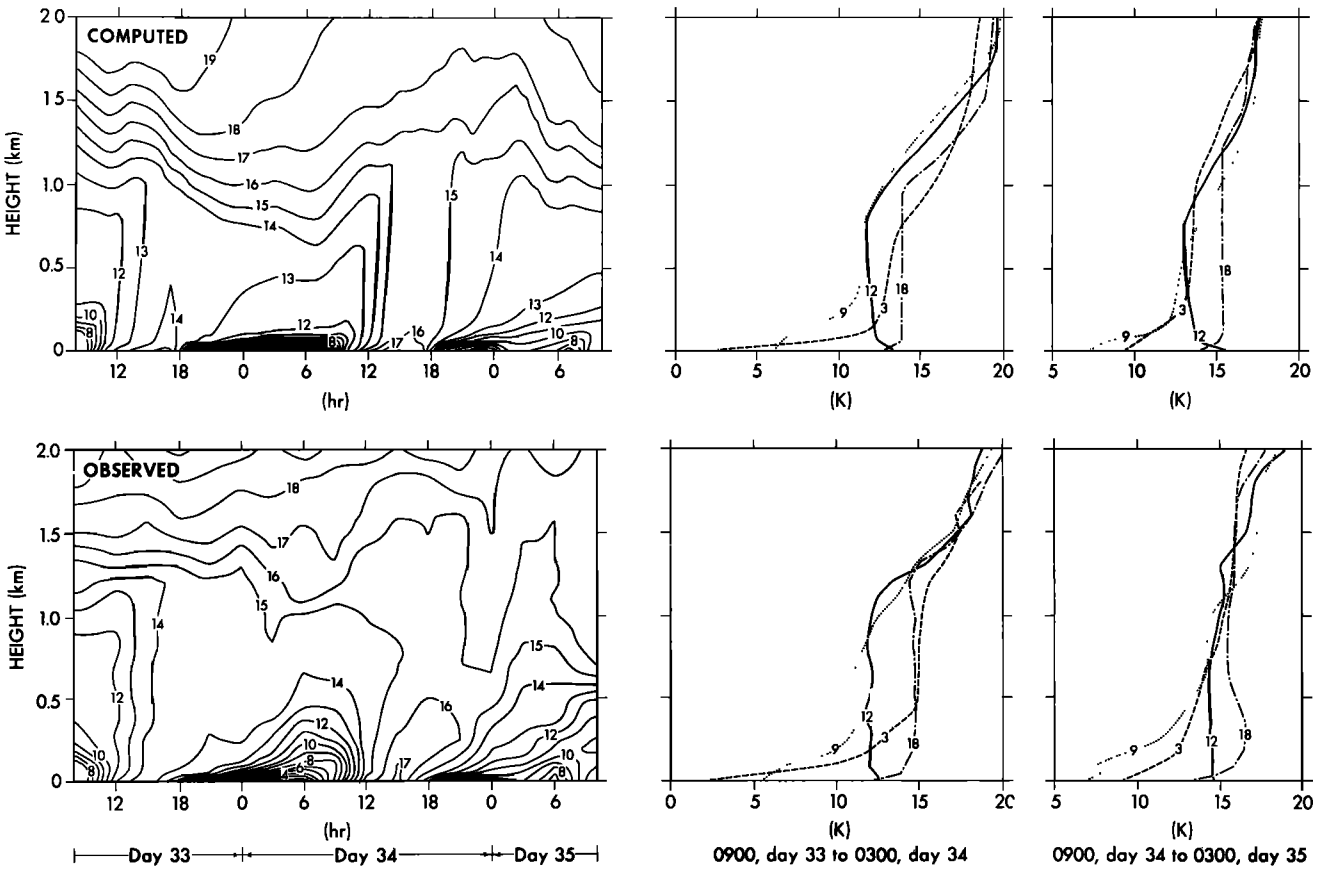

Fig. 11. Observed and calculated atmospheric boundary layer and vertical and temporal variations of mean virtual potential temperature −273°K. Units are degrees Kelvin.

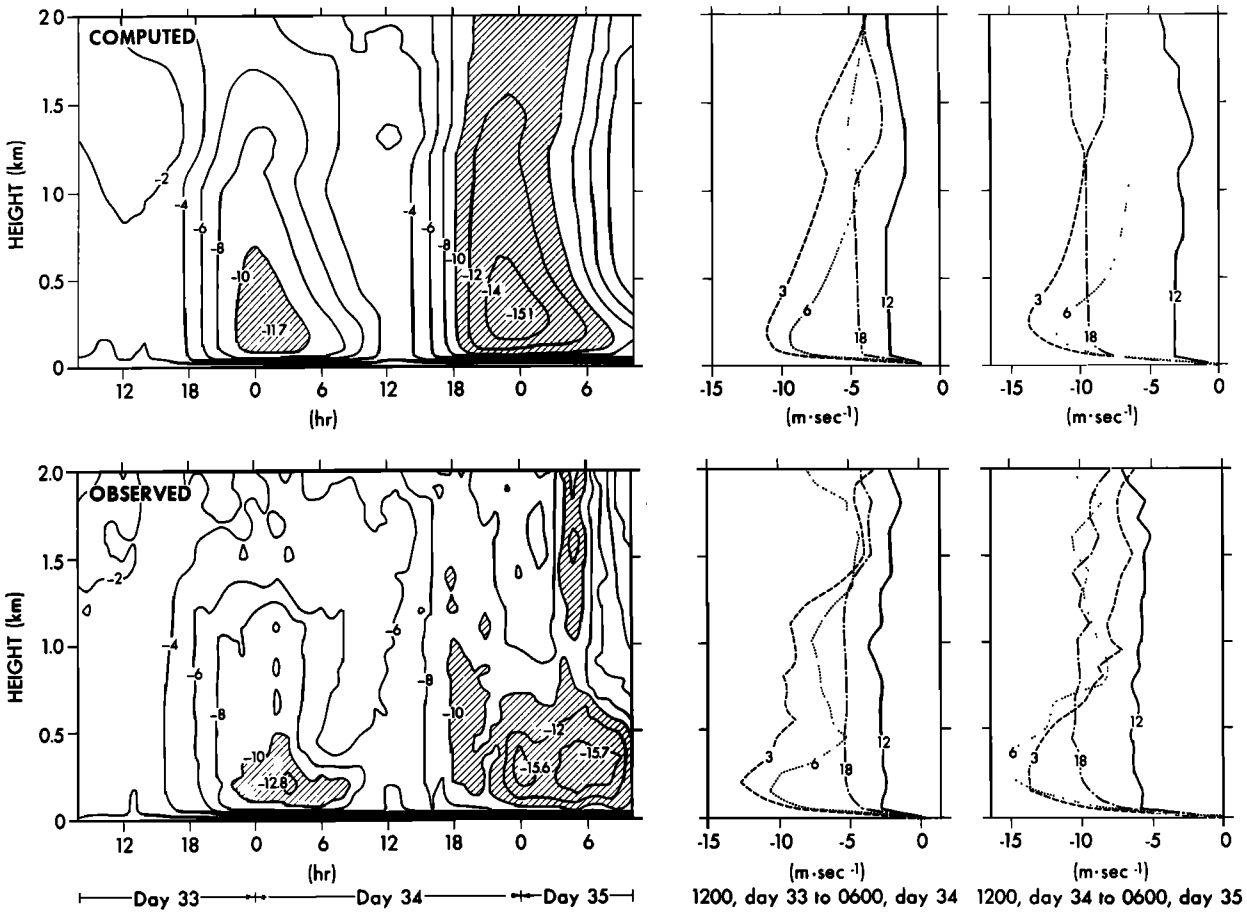

Fig. 12. Observed and calculated atmospheric boundary layer and vertical and temporal variations of the eastward mean wind component. Units are meters per second.

tions shown in these figures used the algebraic length scale equation (50), end of section 6, but we expect the use of (48) would produce little change in the result. The calculations assume horizontal homogeneity so that altitude and time are the only independent variables.

A feature of the velocity field prediction is the appearance of 'the nocturnal wind maximum' around midnight and near $z = 200$ m. The major effect of the diurnal surface heating cycle can best be seen in Figure 14, where we show contours of calculated turbulent kinetic energy. Further details are provided by *Yamada and Mellor* [1975].

Pollutant Dispersion

Model equations developed for temperature may also be applied to any scalar, such as a chemically inert pollutant.

Using the horizontally homogeneous wind field generated for the Wangara simulation, *Yamada* [1977] has made a three-dimensional calculation of the dispersion of a pollutant point source located at various distances from the ground. Figure 15 illustrates the dispersion of a source located at $z = 40$ m during the early morning and afternoon hours. The morning, low-level inversion confines pollutants to near-surface altitudes, whereas vertical mixing in the afternoon is vigorous, as would be deduced from Figure 14. Other calculations, which include an assessment of ground level concentration as influenced by source height, will be found in Yamada's paper.

One finding of interest is that the effect of lateral diffusion terms in the mean concentration equation is negligible except very close to the source. Lateral dispersion is dominated by vertical variability of mean wind speed and direction. Horizontal mean advective dispersion creates mean vertical concentration gradients which are subsequently mixed through vertical diffusion.

Dobosy [1979] has also constructed a two-dimensional (vertical plane) model for pollutant transport based on the level $2\frac{1}{2}$ and 3 models.

Two- and Three-Dimensional Flow With Orography

As a first step toward realistic treatment of terrain effects, the airflow over single and double Gaussian mountains was investigated [*Yamada*, 1978*b*]. The governing equations are transformed into a terrain-following coordinate system in order to simplify the surface boundary conditions. Figure 16*a* shows the horizontal wind vectors 1000 m above the surface of a Gaussian mountain 500 m high. Acceleration and deceleration of the horizontal wind speeds are seen on the lee and upwind sides, respectively. Additionally, the airflow diverges strongly as it approaches the mountain and converges in the lee of the mountain. The covergence and divergence in the horizontal wind fields result in vertical motions computed from the continuity equation. A maximum downward motion of 2 m s^{-1} is obtained approximately 3.5 km above the downwind slope of the mountain; the

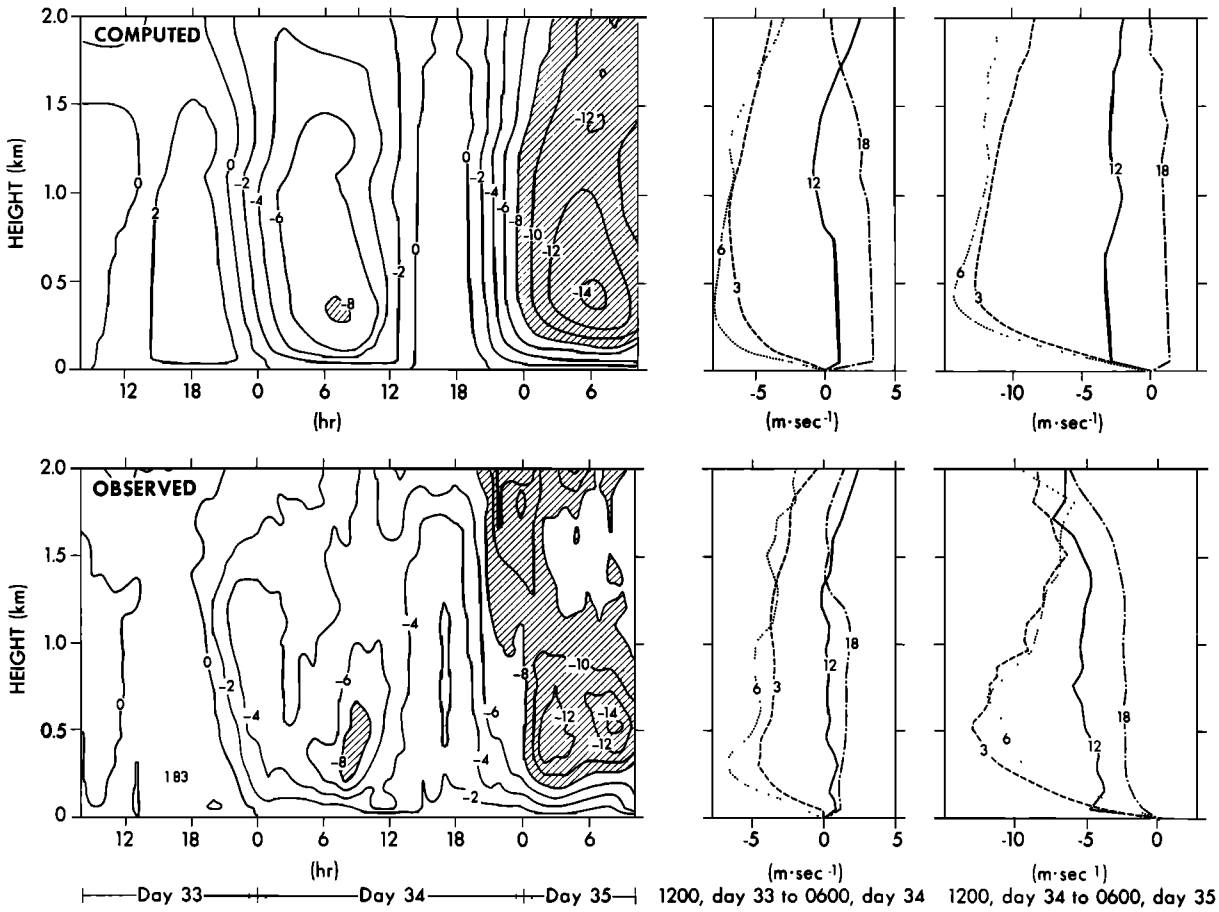

Fig. 13. Observed and calculated atmospheric boundary layer and vertical and temporal variations of the northward mean wind component.

maximum upward motion is only 0.2 m s^{-1}, as upward motion occurs over a greater volume. The potential temperature in a vertical plane through the diagonal A-B in Figure 16*a* is shown in Figure 16*b*. The potential temperature is increased by 8°C in the lee of the peak to subsidence occurring on the lee slope of the mountain. See *Yamada* [1978*b*] for further discussion. Recently, more realistic topography is included in the two-dimensional [*Yamada*, 1982*b*] and three-dimensional [*Yamada*, 1981] models, and the results are compared with observations. Tree canopies are parameterized in a relatively simple manner, but effects of both solar radiation and drag force are properly considered [*Yamada*, 1982*a*].

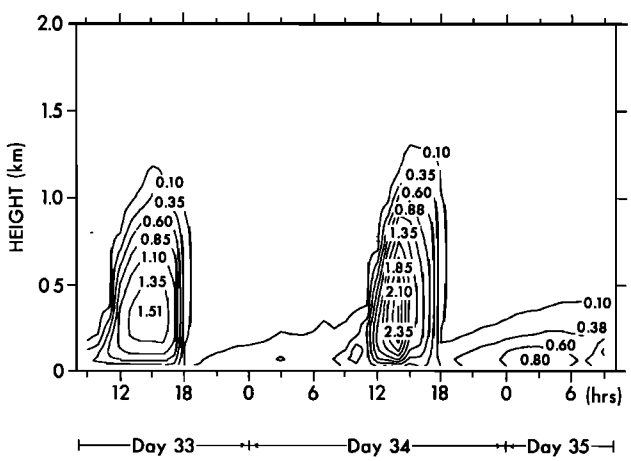

Fig. 14. Time and space variation of computed q^2 (twice the turbulent kinetic energy); units are square meters per second. The stippled areas indicate regions where $10^{-3} < q^2 < 10^{-2}$ m^2 s^{-1}.

Effects of Water Vapor

Exactly the same equations derived in the previous sections are applicable for a moist atmosphere as long as phase changes do not occur and provided that virtual potential temperature $\tilde{\Theta}_v$ defined as

$$\tilde{\Theta}_v = (1 + 0.61\,\tilde{Q}_v)\tilde{\Theta} \tag{56}$$

is everywhere substituted for $\tilde{\Theta}$. In (56), $\tilde{Q}_v$ is the mixing ratio of water vapor, and a tilde indicates an instantaneous value. In all previous equations the mean and the fluctuation of the virtual potential temperature, Θ_v and θ_v, should replace the mean and fluctuation of potential temperature, Θ and θ. In addition, conservation equations of the mean and turbulence fluxes of water vapor can be derived assuming closure assumptions identical to those for the potential temperature are needed to obtain absolute temperature or potential temperature. The resulting equations for the water vapor are also identical in form to those for the potential temperature. Thus, for example, replacing Θ and θ by Q_v and q_v, respectively, in (23), (28), (29), and (31) yields the required equations.

Burk [1977] used the level 3 model to study temporal

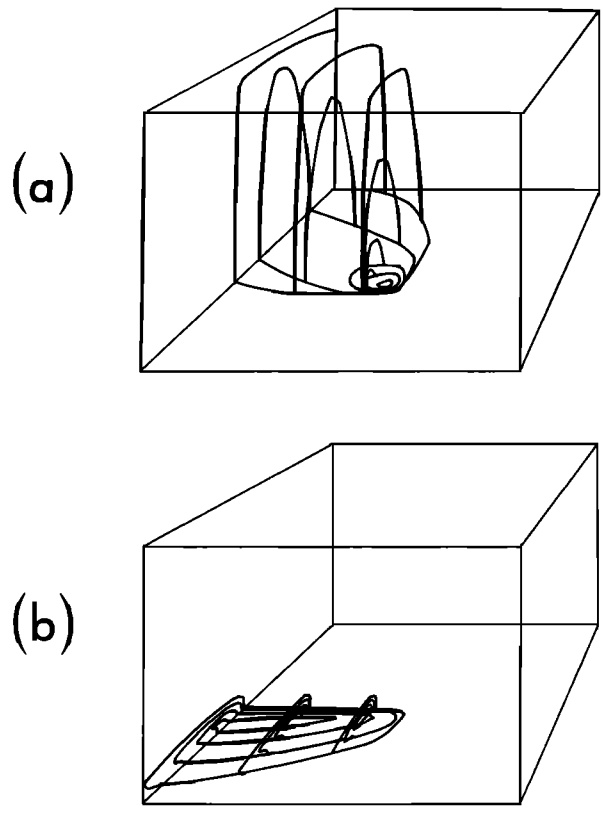

Fig. 15. (*a*) Simulations of pollutant dispersion from a source at 40 m above ground level. The mean wind, temperature, and turbulence field are the same as in Figures 11–14 at 1500 hours on day 33. The box represents a 40 km by 40 km by 1200 m domain. (*b*) Same as Figure 15*a* except the time is 0600 on day 34.

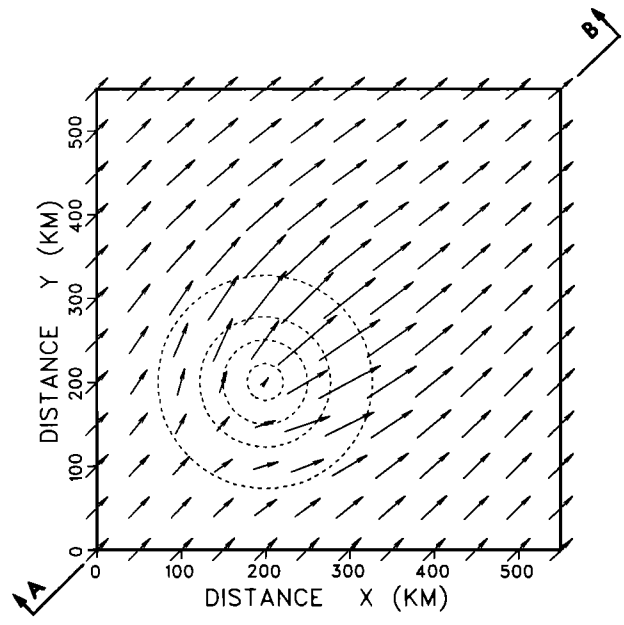

Fig. 16*a*. Horizontal wind vectors at 1000 m above the surface of a mountain in Figure 25. Terrain is contoured by dashed lines with an increment of 150 m. The lowest contour is $z = 20$ m.

variations in the moist atmospheric boundary layer and to investigate mechanisms to explain observations of layers which are well mixed thoroughly but far from well-mixed in terms of moisture.

Condensation

If phase changes occur, however, it becomes rather difficult to solve the equations for the virtual potential temperature and water vapor, since they are not conserved and suitable stipulations of source (sink) terms are not known. Therefore we have taken a different approach. One obviously conserved quantity, even when phase changes occur, is the total water content Q_w, defined as

$$\tilde{Q}_w \equiv \tilde{Q}_v + \tilde{Q}_l \tag{57a}$$

where Q_l is the liquid water. Another conserved quantity used here is the liquid water potential temperature [*Betts*, 1973] $\tilde{\Theta}_l$, defined as

$$\tilde{\Theta}_l \equiv \tilde{\Theta} - \frac{\Theta}{T}\frac{L_v}{C_p}\tilde{Q}_l \tag{57b}$$

where L_v and C_p are the latent heat of evaporation and the specific heat of dry air at constant pressure, respectively. Therefore the conservation equations for the potential temperature as in (23) are replaced by identical equations for the liquid water potential temperature and for total water.

In order to recover the water vapor and absolute temperature fields, which are necessary for determining buoyancy effects on the turbulence and for computing long-wave radiation cooling of the atmosphere, we follow *Sommeria and Deardorff* [1977] and *Mellor* [1977] and assume a joint, Gaussian probability distribution for $\tilde{\Theta}_l$ and $\tilde{Q}_w$. First, however, we will derive equations for the various turbulence moments. The derivation of equations in detail has been already given by *Yamada* [1978*a*] or *Yamada and Mellor* [1979]. Most of the equations for the turbulent moments are similar to those discussed in the previous sections. For example, (26) and (27) remain the same. Equation (28) is virtually the same except that θ is replaced by θ_l so that

$$\begin{aligned}
\langle u\theta_l\rangle &= 3l_2/q\,[-\langle uw\rangle\,\partial\Theta_l/\partial z - \langle w\theta_l\rangle\,\partial U/\partial z] \\
\langle v\theta_l\rangle &= 3l_2/q\,[-\langle vw\rangle\,\partial\Theta_l/\partial z - \langle w\theta_l\rangle\,\partial V/\partial z] \\
\langle w\theta_l\rangle &= 3l_2/q\,[-\langle w^2\rangle\,\partial\Theta_l/\partial z + \beta g\,\langle\theta_v\theta_l\rangle]
\end{aligned} \tag{58}$$

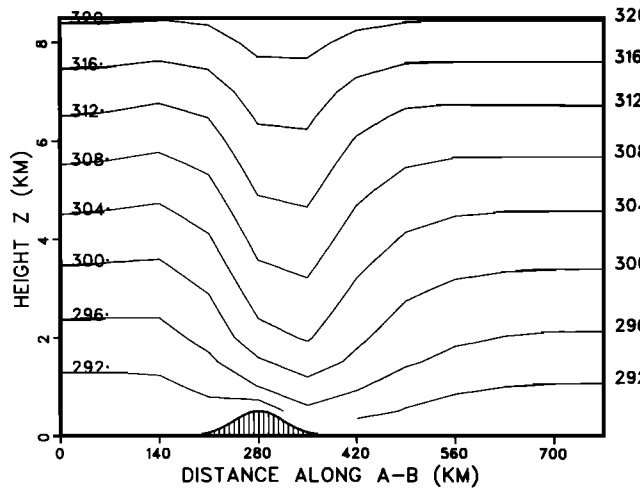

Fig. 16*b*. Distribution of the potential temperature (kelvins) in a vertical plane through the diagonal A-B in Figure 16*a*.

and (29) becomes

$$\langle \theta_l^2 \rangle = -\frac{\Lambda_2}{q} \langle w\theta_l \rangle \frac{\partial \Theta_l}{\partial z} \tag{59}$$

In addition, equations for the fluxes and variance of the total water may be derived, resulting in

$$\begin{aligned} \langle uq_w \rangle &= 3l_2/q\,[-\langle uw \rangle\, \partial Q_w/\partial z - \langle wq_w \rangle\, \partial U/\partial z] \\ \langle vq_w \rangle &= 3l_2/q\,[-\langle vw \rangle\, \partial Q_w/\partial z - \langle wq_w \rangle\, \partial V/\partial z] \\ \langle wq_w \rangle &= 3l_2/q\,[-\langle w^2 \rangle\, \partial Q_w/\partial z + \beta g\, \langle \theta_v q_w \rangle] \end{aligned} \tag{60}$$

and

$$\langle q_w^2 \rangle = -\frac{\Lambda_2}{q} \langle wq_w \rangle \frac{\partial Q_w}{\partial z} \tag{61}$$

Finally, the equation for the cross correlation between θ_l and q_w is

$$0 = -\langle w\theta_l \rangle \frac{\partial Q_w}{\partial z} - \langle wq_w \rangle \frac{\partial \Theta_l}{\partial z} - 2q \frac{\langle \theta_l q_w \rangle}{\Lambda_2} \tag{62}$$

By using (59), (61), and (62) we reduce to the level $2\frac{1}{2}$ model. However, the following condensation physics can be used in the level 4 or 3 models. In particular, *Burk* [1980, 1982] has applied the level 3 model with condensation physics in a study of the turbulence structure parameters which provides useful information in interpreting acoustic optical or microwave propagation measurements.

Unlike the previous cases where phase changes do not occur, the revised set of equations have more unknown terms than the number of equations, because of various correlations involving the fluctuation of virtual potential temperature. Therefore additional expressions to relate these terms $\langle u_j\theta_v \rangle$, $\langle \theta_v\theta_l \rangle$, and $\langle \theta_v q_w \rangle$ to known terms are needed. Readers are again referred to *Yamada* [1978*a*] or *Yamada and Mellor* [1979] for details of derivations. Only a brief discussion and the final results are given here. The virtual temperature relation which includes liquid water is, instead of (56), $\tilde{\Theta}_v = (1 + 0.61\,\tilde{Q}_w - 1.61\,\tilde{Q}_l)\tilde{\Theta}$. Together with (57*b*) we obtain

$$\tilde{\Theta}_v = (1 + 0.61\,\tilde{Q}_w - 1.61\,\tilde{Q}_l)\left(\tilde{\Theta}_l + \frac{\Theta}{T}\frac{L}{C_p}\tilde{Q}_l\right) \tag{63}$$

from which the mean is readily extracted to give

$$\Theta_v = (1 + 0.61\,Q_w - 1.61\,Q_l)\left(\Theta_l + \frac{\Theta}{T}\frac{L}{C_p}Q_l\right) \tag{64}$$

If from (63) and (64) we extract the fluctuating part and take moments, we obtain

$$\beta\langle u_j\theta_v \rangle = \beta_T\langle u_j\theta_l \rangle + \beta_w\langle u_jq_w \rangle + \beta_l\langle u_jq_l \rangle \tag{65a}$$

$$\beta\langle \theta_l\theta_v \rangle = \beta_T\langle \theta_l^2 \rangle + \beta_w\langle \theta_lq_w \rangle + \beta_l\langle \theta_lq_l \rangle \tag{65b}$$

$$\beta\langle q_w\theta_v \rangle = \beta_T\langle q_w\theta_l \rangle + \beta_w\langle q_w^2 \rangle + \beta_l\langle q_wq_l \rangle \tag{65c}$$

where higher-order moments are neglected and

$$\beta_T \equiv \beta(1 + 0.61\,Q_w - 1.61\,Q_l) \tag{66a}$$

$$\beta_l \equiv \beta\left[(1 + 0.61\,Q_w - 3.22\,Q_l)\frac{\Theta}{T}\frac{L_v}{C_p} - 1.61\,\theta_l\right] \tag{66b}$$

$$\beta_w \equiv 0.61\,\beta\left(\Theta_l + \frac{\Theta}{T}\frac{L_v}{C_p}Q_l\right) \tag{66c}$$

We are therefore required to determine $\langle u_jq_l \rangle$, $\langle \theta_lq_l \rangle$, and $\langle q_wq_l \rangle$ to close the equation set. For the latter two quantities, as detailed by *Sommeria and Deardorff* [1977] and *Mellor* [1977], one way is to assume a binormal distribution for θ_l and q_w, which we signify by $G(\theta_l, q_w)$; we also assume 'fast' condensation physics according to $\tilde{Q}_l = (\tilde{Q}_w - \tilde{Q}_s)H(\tilde{Q}_w - \tilde{Q}_s)$, where H is the Heaviside operator and $\tilde{Q}_s$ is the saturation specific humidity value.

Moments are then formed such that

$$R = \int_{-\infty}^{\infty}\int_{-\infty}^{\infty} H(\tilde{Q}_w - \tilde{Q}_s)G(\theta_l, q_w)\,d\theta_l\,dq_w$$

is the cloud fraction and

$$Q_l = \int_{-\infty}^{\infty}\int_{-\infty}^{\infty} (\tilde{Q}_w - \tilde{Q}_s)H(\tilde{Q}_w - \tilde{Q}_s)G(\theta_l, q_w)\,d\theta_l\,dq_w$$

is the mean liquid water. For the turbulent moments,

$$\langle \phi q_l \rangle = \int_{-\infty}^{\infty}\int_{-\infty}^{\infty} \phi q_l\, H(\tilde{Q}_w - \tilde{Q}_s)G(\theta_l, q_w)\,d\theta_l\,dq_w$$

where $\phi = \theta_l$ or q_w. H is zero when $\tilde{Q}_w < \tilde{Q}_s$ and unity when $\tilde{Q}_w > \tilde{Q}_s$, in which case $\tilde{Q}_l = \tilde{Q}_w - \tilde{Q}_s$. In the latter case we expand $\tilde{Q}_s$ in a Taylor series so that it is equated to saturation specific humidity at the mean liquid potential temperature Q_{sl}, plus terms proportional to θ_l and $\tilde{Q}_l$. The result is that the integrals may be worked out and yield

$$R = \tfrac{1}{2}\left[1 + \operatorname{erf}\left\{\frac{a(Q_w - Q_{sl})}{2(2^{1/2})\sigma_s}\right\}\right] \tag{67}$$

$$Q_l = aR(Q_w - Q_{sl}) + \frac{2\sigma_s}{(2\pi)^{1/2}} \exp\left\{-\frac{a^2(Q_w - Q_{sl})^2}{8\sigma_s^2}\right\} \tag{68}$$

$$\frac{\langle \phi q_l \rangle}{a\langle \phi q_w \rangle - b\langle \phi\theta_l \rangle} = R' \equiv R - \frac{Q_l}{2\sigma_s}\frac{1}{(2\pi)^{1/2}} \cdot \exp\left\{-\frac{a^2(Q_w - Q_{sl})^2}{8\sigma_s^2}\right\} \tag{69}$$

where $\phi = \theta_l$ or q_w. The parameters a, b, and σ_s are

$$a \equiv \left[1 + Q_{sl,T}\frac{L}{C_p}\right]^{-1} \tag{70a}$$

$$b \equiv a(T/\theta)Q_{sl,T} \tag{70b}$$

$$\sigma_s^2 = \tfrac{1}{4}\,(a^2\langle q_w^2 \rangle - 2ab\langle q_w\theta_l \rangle + b^2\langle \theta_l^2 \rangle) \tag{70c}$$

$Q_{sl,T}$ is obtained from the Clasius-Clapeyron equation and is the derivative of the saturation specific humidity with respect to temperature and evaluated at the mean liquid potential temperature.

By assuming a trinormal probability distribution which includes as arguments u_j as well as θ_l and q_w, it may be shown that (69) is also valid where $\phi = u_j$.

With the use of the flux equations and (59), (61), and (62), equation (70*c*) may be written in the following, computationally convenient form:

$$\sigma_s^2 = \frac{\Lambda_2}{4q} K_H \left(b\frac{\partial \theta_l}{\partial z} - a\frac{\partial Q_w}{\partial z}\right)^2 \tag{71}$$

Now successively inserting $\phi = u_j$, θ_l, and q_w into (69) provides necessary moments for insertion into (65*a*)–(65*c*). The results for $\langle u_j\theta_v\rangle$, $\langle\theta_l\theta_v\rangle$, and $\langle q_w\theta_v\rangle$ are then used in (58), (60), and (62). The expression for $\langle w\theta_v\rangle$ for use in (25*b*) becomes

$$\beta\langle w\theta_v\rangle = (\beta_T - \beta_l R'b)\langle w\theta_l\rangle + (\beta_w + \beta_l R'a)\langle wq\rangle \qquad (72)$$

Finally, these results may be cast in the form of (30*a*), (30*b*), and (31) where, however, we write $\langle\theta_l w\rangle$ and Θ_l in place of $\langle\theta w\rangle$ and Θ and add a flux equation for $\langle qw\rangle$,

$$-\langle wq_w\rangle = K_H\,\partial Q_w/\partial z \qquad (73)$$

Equations (33*a*), (34), (35), and (36) remain unchanged except for the fact that G_H must be redefined so that

$$G_H = -(l^2/q^2)\,\beta g\zeta \qquad (74a)$$

where ζ is defined by

$$\zeta \equiv (\beta_T - \beta_l R'b)\frac{\partial\theta_l}{\partial z} + (\beta_w + \beta_l R'a)\frac{\partial Q_w}{\partial z} \qquad (74b)$$

It is useful to note that as $\sigma_s \to 0$, the above formulism reverts to a simple condensation model involving only mean quantities. Since it may be shown that $a(Q_w - Q_{sl}) = Q_w - Q_s$, we obtain $R = H(Q_w - Q_s)$ and $Q_l = (Q_w - Q_s)H(Q_w - Q_s)$ as $\sigma_s \to 0$, where, once again, H is the Heaviside operator.

Cloud Simulation

The application of the cloud model is still very much in a research stage, and development is handicapped by lack of data. However, a one-dimensional version of the present set of equations including condensation processes was used to simulate the Barbados Oceanographic and Meteorological Experiment (BOMEX) data [*Holland and Rasmusson*, 1973]. Model results and comparison with available data were discussed in detail by *Yamada and Mellor* [1979]. The BOMEX was conducted over and in the tropical ocean near the island of Barbados. The vertical profiles of computed and observed mean wind speeds, water vapor, and virtual temperature agreed reasonably well and are not shown. The results of the model-computed profiles of some turbulence variables, the mean and variance of liquid water, and cloud volume are shown in Figure 17. No data were available for quantitative comparison of these variables. Satellite photographs, however, indicate that the computed cloud volumes were slightly overestimated. One interesting result is seen in the vertical profiles of the computed turbulence energy and eddy viscosity in Figure 17. These variables exhibit several maxima in the layers 1–3 km above the surface. Increases of the computed turbulence energy and eddy viscosity are closely related with the increases of the liquid water. The condensation process releases latent heat which produces locally unstable layers, resulting in larger turbulence.

Cooling Pond Simulation

A three-dimensional version of the model developed here has been used by *Yamada* [1978*a*, 1979] to evaluate quantitatively the effects of a large cooling pond on the surrounding environment. The time dependent equations were integrated to obtain a nearly stationary state of the circulation over a 2 km by 2 km square pond. Typical values observed for the wind speed, temperature, relative humidity in the surface layer, and water surface temperature were used to construct initial values and boundary conditions. The water and land temperatures were kept constant throughout the integration at 18°C and −10°C, respectively. Figure 18*a* shows the computed horizontal surface wind vectors at 0.2 m above the surface. Wind speeds increased from 1.4 m s^{-1} at the inflow boundary to 3.8 m s^{-1} over the cooling pond. This acceleration of wind speed is caused by the decrease of roughness length over land (3×10^{-2} m is assumed) to that over water

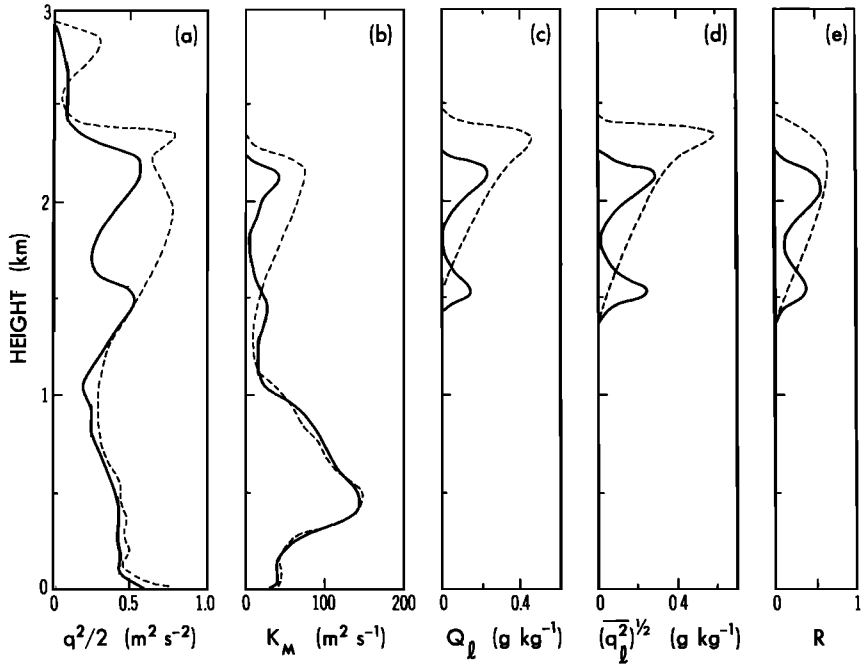

Fig. 17. BOMEX cloud simulation. (*a*) Simulated turbulence energy, (*b*) viscosity coefficients, (*c*) mixing ratio of liquid water, (*d*) rms of the variance of liquid water, and (*e*) cloud fraction. Solid lines are for 0600 hours and dashed lines for 1500 hours on June 24.

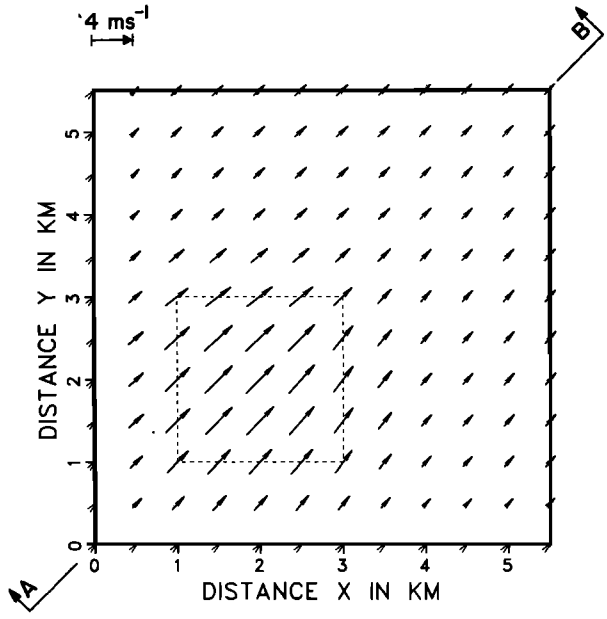

Fig. 18*a*. Horizontal wind vectors at 0.2 m above the surface. The boundary of the cooling pond is indicated by dashed lines.

(5×10^{-5} m, a typical value computed from $0.16u_\tau^2/g$, where u_τ is a friction velocity) and by the air circulation induced by the temperature difference between the land and the pond. Convergence and divergence in the horizontal wind distributions result in the vertical wind distribution (Figure 18*b*) in a vertical plane. A maximum upward motion of 3.5 cm s^{-1} is computed over the downstream edge of the cooling pond.

Global Atmospheric Simulations

The level $2\frac{1}{2}$ model, with the algebraic length scale equation described previously, has now been incorporated into the general circulation models of the National Oceanographic and Atmospheric Administration's Geophysical Fluid Dynamics Laboratory. Currently, one such model represents the global atmosphere with horizontal resolution of about 4° latitude and longitude and 18 vertical levels; the first five levels are assigned to the lower 2 km.

These calculations produce an enormous amount of numbers. Calculations extracted from a paper by *Miyakoda and Sirutis* [1977] are shown in Figure 19. They are zonally averaged plots of temperature, zonal velocity, and $K_M \equiv lq$

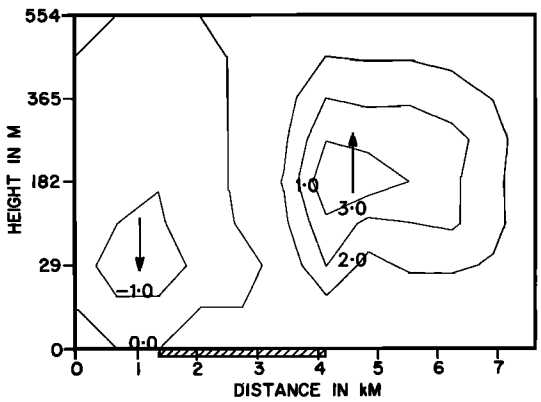

Fig. 18*b*. Distribution of W in a vertical plane through the diagonal A-B shown in Figure 18*a*. Units are centimeters per second.

S_M. Synoptic detail is therefore averaged out of the plots. Nevertheless, one can identify the troposphere, tropopause, and stratosphere in Figure 19*a*; in Figure 19*b* the jet streams are evident.

Oceanographic Simulations

The models we have described have been applied to oceanographic problems. The effect of salinity can be incorporated in, say, the level $2\frac{1}{2}$ model by simply setting $\beta\langle w\theta_v\rangle = \beta_\theta\langle w\theta\rangle + \beta_s\langle ws\rangle$, where $\langle w\theta\rangle$ is the potential temperature flux and $\langle ws\rangle$ is the salinity flux; β_θ and β_s are the corresponding coefficients of thermal expansion. It can be shown that K_H obtained in (32*b*) applies to both potential temperature and salinity. Furthermore, (34) and (35) are unchanged so long as $\beta\,\partial\Theta_v/\partial z = \beta_\theta\,\partial\Theta/\partial z + \beta_s\,\partial S/\partial z$ in (33*b*).

The level 2 model was applied by *Mellor and Durbin* [1975] to ocean mixed layers and seemed to perform well with respect to laboratory simulations and also seemed to simulate data obtained at station PAPA in the North Pacific.

It has been applied by *Weatherly and Martin* [1978] to the study of ocean bottom layers and by *Adams and Weatherly* [1981] to the study of bottom sediment transport. *Simons* [1980] has used the model to hindcast the seasonal variation of horizontally averaged temperature profiles in Lake Ontario using measured winds and storage-derived surface heat flux. The calculated temperature profiles were in close agreement with observation. A similar study was made by *Klein* [1980], and agreement was obtained with wind-driven mixed layer deepening data obtained in the Mediterranean. *Klein* [1980] also performed several useful sensitivity studies concerning the effect of wind-forcing frequencies. Mixed layers when forced with the resonant, inertial frequency will deepen much faster than when forced with higher or lower frequencies.

A paper by *Clancy and Martin* [1981] presages the role of turbulent closure models in operationally forcasting the properties of ocean surface mixed layers. They also used the simplest level 2 model. One of their conclusions is that forecast errors are more associated with initialization fields (combining climatology and expendable bathythermograph drops where available) and surface boundary conditions (derived from the Navy's meteorological model) than with inadequacy of model physics. Further discussion of the needs and potential for operational ocean forecasting can be found in the work by *Elsberry and Garwood* [1980]. *Garwood* [1979] has also made available a general review of mixed layer dynamics and mixed layer models.

More recently, the level $2\frac{1}{2}$ model has been applied to three-dimensional ocean simulation by *Blumberg and Mellor* [1980]. However, some two-dimensional (x, z) calculations were also included in their paper. Thus Figures 20 and 21 illustrate the results of an impulsively imposed alongshore wind stress. Figure 20 is a homogeneous upwelling event, whereas Figure 21 is a density-stratified upwelling event. The role of stratification in confining mixing to surface and bottom layers is readily apparent. Also, in Figure 21, one will observe the formation of a nearshore (x = 2 km) front and baroclinic jet. *Foo* [1981] has presented a more comprehensive study of nearshore upwelling and frontogenesis using a level $2\frac{1}{2}$ model.

It should be noted that in this application the master length scale equation (48) works quite well. It is integrated throughout the entire computational domain and yields both surface

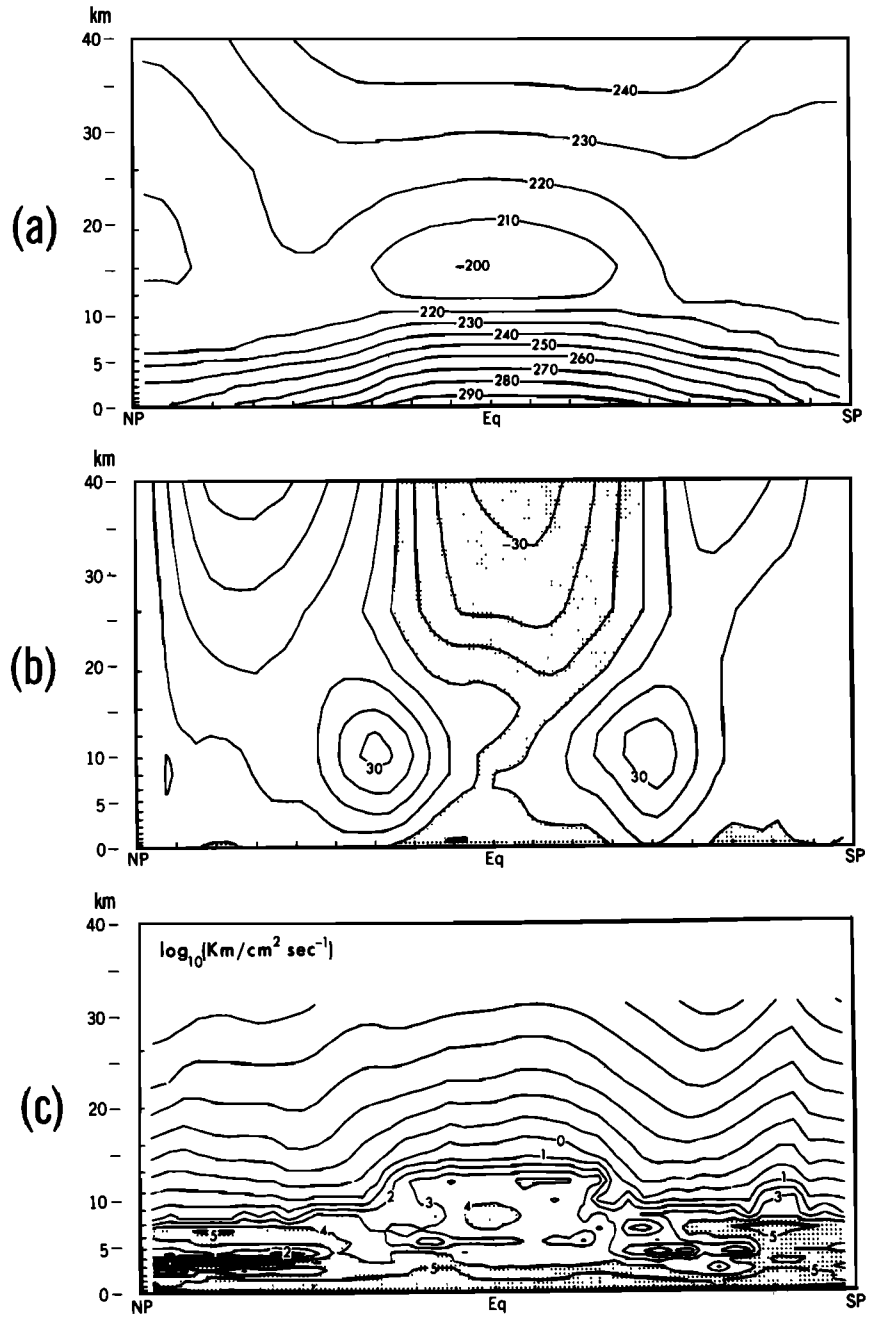

Fig. 19. Zonally averaged variable contours from the global atmospheric simulation by *Miyakoda and Sirutis* [1977] in March. (*a*) Virtual potential temperature. Units are degrees Kelvin. (*b*) Eastward velocity contours. Units are meters per second. (*c*) Log_{10} of $K_M/(\text{cm}^2\ \text{s}^{-1})$.

layer and bottom layer master lengths appropriate to each layer.

Figure 22 shows comparison between observed temperature data and calculation for the annual cycle in upper layers. The observed data are the climatological temperature profiles in the Gulf of Mexico. Data from hydrographic surveys are averaged by month. The data are then area-averaged throughout the basin. Salinity profiles are also obtained but play a minor dynamical role in the Gulf. The model is driven by winds obtained from ship reports and averaged in a similar fashion. Drag coefficients very close to those recommended by *Bunker* [1976] were used to obtain surface stress statistics $\bar{\tau}_x$, $\bar{\tau}_y$, and $|\bar{\tau}|$, where the overbar here represents the average of all data in a given month and on an average. The actual imposed wind stress oscillates (with a 4-day period) in magnitude and direction so that the resulting $\bar{\tau}_x$, $\bar{\tau}_y$, and $|\bar{\tau}|$ match the data. The imposed surface heat flux was simply extracted from the data so that the heat storage (vertical integral of temperature) of the calculation and data agree. (Note that for the same heat storage many profiles are possible including, at one extreme, very large summertime temperature confined to a very thin surface layer.) The final result is that observationally predicted temperature profiles compare quite well. Further details and an account of a fully three-dimensional model as applied to the Gulf of Mexico are found in a report by *Blumberg and Mellor* [1981].

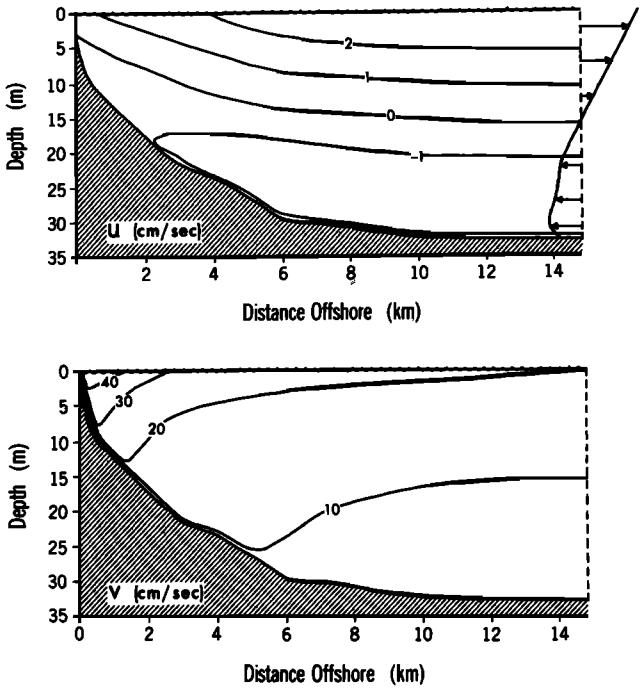

Fig. 20. A homogeneous upwelling event induced by an alongshore wind stress of 2.0 dyn/cm^2 directed into the plane of the paper. The wind stress has been imposed for 6 hours. The onshore (U negative) and offshore (U positive) isotachs are depicted in the upper portion of the figure, while the alongshore (V positive into the plane of the paper, V negative out of the plane of the paper) isotachs are depicted in the lower portion.

9. Discussion

A turbulence model has been developed which is relatively simple and which can be applied to a wide variety of engineering and geophysical flows.

We separate the study of the model into (1) the group of closure assumptions proposed by Rotta, extended to include temperature (or any other scalar) and density stratification, and (2) the master length scale.

The rules of the game we are playing, at least until the present, are to obtain all empirical constants from neutral data and then see if the model can predict stabilization or destabilization of turbulent fields due to density stratification in a gravity field and, in separate studies, due to flow curvature and other body force–like effects. The constants in (12), one of which is not independent, are unambiguously related to simple neutral flow data, and computer solutions are not required to identify these constants. The remaining constants are von Karman's constant κ and the three constants in (48), one of which is not independent. Trial and error computer solutions have determined these last two independent constants.

The model and the fixed set of constants seem to perform well in predicting diverse neutral flows. The same model, with no alteration, appears to predict density-stratified flows in a manner which far exceeds expectation prior to 1973.

The various models, levels 4, 3, $2\frac{1}{2}$, and 2, represent decreasing complexity and decreasing requirements for computer time and storage. For one- (vertical) and perhaps two-dimensional model simulations, any version is affordable. However, for large, three-dimensional, atmospheric or oceanographic numerical models the level 4, certainly, and the level 3, probably, must yield to either the level $2\frac{1}{2}$ or the level 2 closure model on the basis of computational economics.

The level 2 model has received the greatest exposure in the literature, partly because of computer economy and partly because it is relatively easy to program. For most of our own work we use the level $2\frac{1}{2}$ model. This requires the solution of equations for q^2 and q^2l, over and above the usual prognostic equations for mean velocity, temperature, and

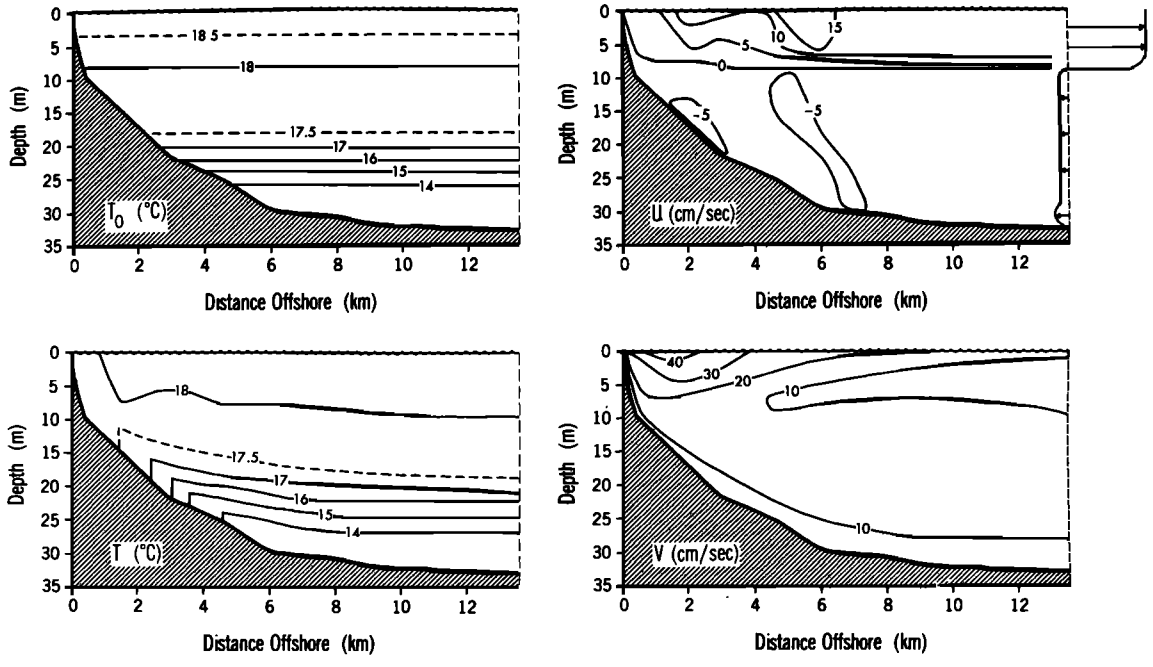

Fig. 21. A stratified upwelling event induced by an alongshore wind stress of 1.0 dyn/cm directed into the plane of the paper. This wind stress has been imposed for 12 hours. The direction of the isotachs is the same as in Figure 20. The initial temperature distribution is denoted as T_0.

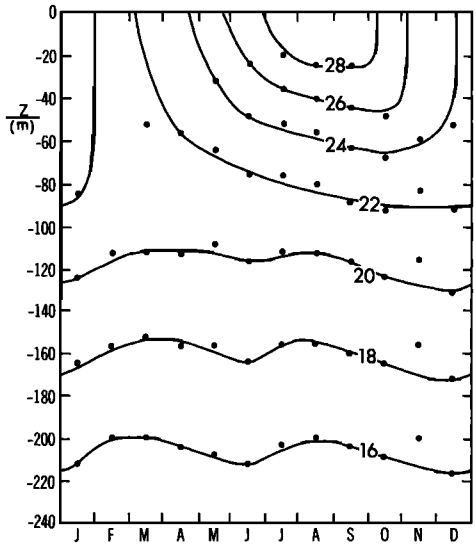

Fig. 22*a*. The climatological, area-averaged time-depth variation of temperature in the Gulf of Mexico.

humidity for the atmosphere or salinity for the ocean. It has a greater predictive range than the level 2 model, and the length scale equation, although the most empirical element of the complete model, does seem to perform in a more satisfactory manner than the simple algebraic equation associated with the level 2 model. For example, in ocean simulations, all equations may be integrated top to bottom and generally include separate, surface and bottom mixed layers bounding nonturbulent flow. The prototype example of a single boundary layer bounded by nonturbulent flow is the laboratory flow in Figure 7. On the other hand, in shallow water, where surface and bottom layers merge, the length scale equation performs well, as was seen in the prototypical merged layer case of channel flow in Figure 6.

It is important to realize that the simpler models cannot, in principle, account for some flow behavior. For example, Uberoi's experiment requires the full level 4 model to account for the return to isotropy for a homogeneous, initially anisotropic flow field where shear and buoyancy production are nil. The levels 3 and $2\frac{1}{2}$ models will correctly account for the decay of turbulent kinetic energy, but all energy components will be declared equal. Finally, the level 2 model, for the same flow, will yield zero turbulent kinetic energy. Since spatial diffusion of energy is lacking, it will also yield zero turbulent kinetic energy at the center line of channel flow, contrary to observation. Nevertheless, in many geophysical applications the level 2 model works quite well, since mixing events are generally dominated by the shear or buoyancy production terms in the turbulent kinetic energy equation.

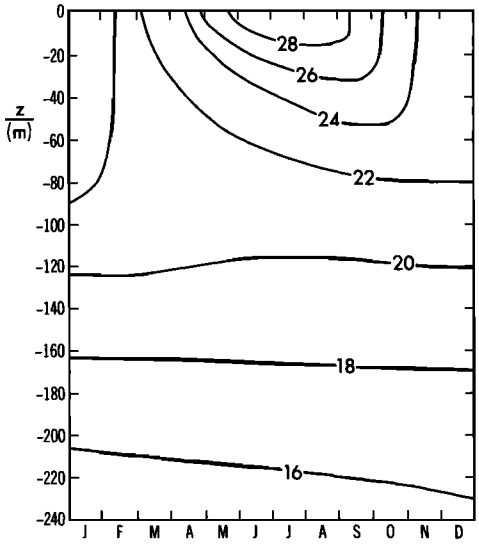

Fig. 22*b*. Model simulation of the time-depth variation of temperature in the Gulf of Mexico.

Acknowledgments. This research was supported by the Air Force Office of Scientific Research under grant AFOSR 79-0118, by the National Oceanic and Atmospheric Administration under grant 04-7-022-44017 (G.L.M.), and by the U.S. Department of Energy's ASCOT program (T.Y.).

REFERENCES

Adams, C. E., Jr., and G. L. Weatherly, Some effects of suspended sediment stratification on an oceanic bottom boundary layer, *J. Geophys. Res., 86,* 4161–4172, 1981.

Andre, J. C., G. DeMoor, P. Lacarrere, and R. Du Vachat, Turbulence approximation for inhomogeneous flows, I, The clipping approximation, *J. Atmos. Sci., 33,* 476–481, 1976*a*.

Andre, J. C., G. DeMoor, P. Lacarrere, and R. Du Vachat, Turbulence approximation for inhomogeneous flows, II, The numerical simulation of a penetrative convection experiment, *J. Atmos. Sci., 33,* 482–491, 1976*b*.

Betts, A. K., Non-precipitating cumulus convection and its parameterization, *Q. J. R. Meteorol. Soc., 99,* 178–179, 1973.

Blumberg, A. F., and G. L. Mellor, A coastal ocean numerical model, in *Proceedings of the Symposium on Mathematical Modelling of Estuarine Physics,* Springer-Verlag, New York, 1980.

Blumberg, A. F., and G. L. Mellor, A numerical calculation of the circulation in the Gulf of Mexico, *Rep. 66,* 153 pp., Dynalsis of Princeton, Princeton, N. J., 1981.

Bremhorst, K., and K. J. Bullock, Spectral measurements of turbulent heat and momentum transfer in fully developed pipe flow, *Int. J. Heat Mass Transfer, 16,* 2141–2154, 1973.

Briggs, M., G. Mellor, and T. Yamada, A second moment turbulence model applied to fully separated flow, in *Proceedings: 1976 SQUID Workshop on Turbulence in Internal Flows,* pp. 249–276, Hemisphere, Washington, D. C., 1976.

Bunker, A. F., Computation of surface energy flux and air-sea interaction cycles of the North Atlantic Ocean, *Mon. Weather Rev., 104,* 1122–1139, 1976.

Burk, S. D., The moist boundary layer with a higher order turbulence closure model, *J. Atmos. Sci., 34,* 629–638, 1977.

Burk, S. D., Refractive index structure parameters: Time-dependent calculations using a numerical boundary-layer model, *J. Appl. Meteorol., 19,* 562–576, 1980.

Burk, S. D., Comparison of structure parameter scaling expression with turbulence closure model predictions, *J. Atmos. Sci., 38,* 751–761, 1981.

Businger, J. A., J. C. Wyngaard, Y. Izumi, and E. F. Bradley, Flux profile relationships in the atmospheric surface layer, *J. Atmos. Sci., 28,* 181–189, 1971.

Caughey, S. J., and J. C. Wyngaard, The turbulence kinetic energy budget in convective conditions, *Q. J. R. Meteorol. Soc., 105,* 231–239, 1979.

Champagne, F. H., V. G. Harris, and S. Corrsin, Experiments on nearly homogeneous turbulent shear flow, *J. Fluid Mech., 41,* 81–141, 1970.

Clancy, R. M., and P. J. Martin, Synoptic forecasting of the oceanic mixed layer using the Navy's operational environmental data base: Present capabilities and future applications, *Bull. Am. Meteorol. Soc., 62,* 770–784, 1981.

Clarke, R. W., A. Dyer, R. R. Brook, D. G. Reid, and A. J. Troup, The Wangara experiment: Boundary layer data, *Tech. Pap. 19,*

Div. of Meteorol. Phys., Commonwealth Sci. and Ind. Res. Organ., Melbourne, Australia, 1971.

Comte-Bellot, G., Ecoulement turbulent entre deax parois parelleles, *Publ. Sci. Tech. 419,* Ministère de l'Air, Paris, 1965.

Daly, B. J., and F. H. Harlow, Transport equations in turbulence, *Phys. Fluids, 13,* 2634–2649, 1970.

Deardorff, J. W., Three dimensional numerical study of turbulence in an entraining mixed layer, *Boundary Layer Meteorol., 7,* 199–226, 1974.

Dickey, T. D., and G. L. Mellor, Decaying turbulence in neutral and stratified fluids, *J. Fluid Mech., 99,* 13–31, 1980.

Dobosy, R., Dispersion of atmospheric pollutants in flow over the shorelines of a large body of water, *J. Appl. Meteorol., 18,* 117–132, 1979.

Donaldson, C. D., and H. Rosenbaum, Calculation of the turbulent shear flows through closure of the Reynolds equations by invariant modeling, *ARAP Rep. 127,* Aeronaut. Res. Assoc. of Princeton, Princeton, N. J., 1968.

Elsberry, R. L., and R. W. Garwood, Numerical ocean prediction models—Goal for the 1980's, *Bull. Am. Meteorol. Soc., 61,* 1556–1566, 1980.

Foo, E.-C., A two-dimensional diabatic isopycnal model simulating the coastal upwelling front, *J. Phys. Oceanogr., 11,* 604–626, 1981.

Gambo, K., Notes on the turbulence closure model for atmospheric boundary layer, *J. Meteorol. Soc. Jpn., 56,* 466–480, 1978.

Garwood, R. W., Jr., Air-sea interactions and dynamics of the surface mixed layer, *Rev. Geophys. Space Phys., 17,* 1507–1524, 1979.

Gibson, C. H., and W. H. Schwartz, The universal spectra of turbulent velocity and scalar fields, *J. Fluid Mech., 16,* 365–384, 1965.

Gowen, K. A., and J. W. Smith, Turbulent heat transfer from smooth and rough surfaces, *Int. J. Heat Mass Transfer, 11,* 1657–1673, 1968.

Hanjalic, K., and B. E. Launder, Fully developed asymmetric flow in a plane channel, *J. Fluid Mech., 52,* 689, 1972.

Harsha, P. T., Kinetic energy methods, in *Handbook of Turbulence,* edited in W. Frost and T. H. Moulden, pp. 187–232, Plenum, New York, 1977.

Hinze, J. O., *Turbulence,* 790 pp., McGraw-Hill, New York, 1975.

Holland, J. Z., and E. M. Rasmusson, Measurements of the atmospheric, mass, energy and momentum budget over a 500-kilometer square of tropical ocean, *Mon. Weather Rev., 101,* 44–45, 1973.

Kantha, L. H., O. M. Phillips, and R. S. Azad, On the turbulent entrainment at a stable density interface, *J. Fluid Mech., 79,* 753–758, 1977.

Kato, H., and O. M. Phillips, On the penetration of a turbulent layer into a stratified fluid, *J. Fluid Mech., 37,* 643–655, 1969.

Kestin, J., and P. D. Richardson, Heat transfer across turbulent incompressible boundary layers, in *Colloque International sur la Mécanique de la Turbulence, Marseille,* Editions du Centre National de la Recherche Scientifique, Paris, 1961.

Klebanoff, P. S., Characteristics of turbulence in a boundary layer with zero pressure gradient, *Rep. 1247,* Natl. Adv. Comm. for Aeronaut., Washington, D. C., 1955.

Klein, P., A simulation of the air-sea transfer variability on the structure of marine upper layers, *J. Phys. Oceanogr., 10,* 1824–1841, 1980.

Kline, S. J., M. V. Morkovin, G. Sovran, and D. J. Cockrell, in *Proceedings of the AFOSR Stanford Conference on Computation of Turbulent Boundary Layers,* Thermosciences Division, Department of Mechanical Engineering, Stanford University, Stanford, Calif., 1968.

Kolmogorov, A. N., The local structure of turbulence in incompressible viscous fluid for very large Reynolds number (in Russian), *Dokl. Akad. Nauk SSSR, 30,* 301, 1941. (English translation, S. K. Friedlander and L. Topper, *Turbulence,* Interscience, New York, 1961.)

Kukharets, V. P., and L. R. Tsvang, The turbulent energy dissipation rate in an unstable stratified atmospheric boundary layer, *Izv. Acad. Sci. USSR Atmos. Oceanic Phys.,* Engl. Transl., *13,* 419–424, 1977.

Laufer, J., Investigation of turbulent flow in a two-dimensional channel, *Tech. Note 2123,* Natl. Adv. Comm. for Aeronaut., Washington, D. C., 1950.

Laufer, J., The structure of turbulence in fully developed pipe flow, *Rep. 1174,* Natl. Adv. Comm. for Aeronaut., Washington, D. C., 1954.

Launder, B. E., On the effect of a gravitational field on the turbulent transport of heat momentum, *J. Fluid Mech., 67,* 569–581, 1975.

Launder, B. E., G. J. Reece, and W. Rodi, Progress in the development of a Reynolds-stress turbulence closure, *J. Fluid Mech., 68,* 537–566, 1975.

Lenschow, D. J., Airplane measurements of planetary boundary layer structure, *J. Appl. Meteorol., 9,* 874–884, 1970.

Lewellen, W. S., Use of invariant modelling, in *Handbook of Turbulence,* edited by W. Feast and T. H. Moulden, pp. 237–277, Plenum, New York, 1977.

Lewellen, W. S., and M. E. Teske, Prediction of the Monin-Obukhov similarity functions from an invariant model of turbulence, *J. Atmos. Sci., 30,* 1340–1345, 1973.

Lewellen, W. S., M. E. Teske, and C. D. Donaldson, Variable density flows computed by a second-order closure description of turbulence, *AIAA J., 14,* 382–387, 1976.

Lumley, J. L., and B. Khajeh-Nouri, Modeling homogeneous deformation of turbulence, *Adv. Geophys., 18A,* 162–192, 1974.

Lumley, J. L., O. Zeman, and J. Seiss, The influence of buoyancy on turbulent transport, *J. Fluid Mech., 84,* 581–597, 1978.

Mellor, G. L., The large Reynolds number asymptotic theory of turbulent boundary layers, *Int. J. Eng. Sci., 11,* 851–873, 1972.

Mellor, G. L., Analytic prediction of the properties of stratified planetary surface layers, *J. Atmos. Sci., 30,* 1061–1069, 1973.

Mellor, G. L., A comparative study of curved flow and density, stratified flow, *J. Atmos. Sci., 32,* 1278–1282, 1975.

Mellor, G. L., The Gaussian cloud model relation, *J. Atmos. Sci., 34,* 356–358, 1977. (Corrigenda, *J. Atmos. Sci., 34,* 1483–1484, 1977.)

Mellor, G. L., and P. A. Durbin, The structure and dynamics of the ocean surface mixed layer, *J. Phys. Oceanogr., 5,* 718–728, 1975.

Mellor, G. L., and H. J. Herring, A survey of the mean turbulent field closure models, *AIAA J., 11,* 590–599, 1973.

Mellor, G. L., and P. T. Strub, Similarity solutions for the stratified turbulent Rayleigh problem, *J. Phys. Oceanogr., 10,* 455–460, 1980.

Mellor, G. L., and T. Yamada, A hierarchy of turbulence closure models for planetary boundary layers, *J. Atmos. Sci., 31,* 1791–1806, 1974. (Corrigenda, *J. Atmos. Sci., 34,* 1482, 1977.)

Miyakoda, K., and J. Sirutis, Comparative integrations of global models with various parameterized processes of sub-grid scale vertical transports, *Contrib. Atmos. Phys., 50,* 445–447, 1977.

Monin, A. S., On the symmetry properties of turbulence in the surface layers of air, *Izv. Acad. Sci. USSR Atmos. Oceanic Phys.,* Engl. Transl., *1,* 45–54, 1965.

Ng, K. E., and D. B. Spalding, Turbulence model for boundary layers near walls, *Phys. Fluids, 15,* 20–30, 1972.

Pennel, W. T., and M. A. LeMone, An experimental study of turbulence structure in the fair-weather trade wind boundary layer, *J. Atmos. Sci., 31,* 1308–1323, 1974.

Perry, A. E., and C. J. Abell, Scaling laws for pipe-flow turbulence, *J. Fluid Mech., 67,* 257–271, 1975.

Rose, W. G., Results of an attempt to generate a homogenous turbulent shear flow, *J. Fluid Mech., 67,* 257–271, 1966.

Rotta, J. C., Statistische Theorie nichthomogener Turbulenz, 1, *Z. Phys. 129,* 547–572, 1951*a*.

Rotta, J. C., Statistische Theorie nichthomogener Turbulenz, 2, *Z. Phys.,* 131, 51–77, 1951*b*.

Rotta, J. C., Turbulent shear layer prediction on the basis of the transport equations for the Reynolds stresses, in *Proceedings of the 13th International Congress on Theoretical and Applied Mechanics, Moscow University,* pp. 295–308, Springer-Verlag, New York, 1973.

Shir, C. C., A preliminary study of atmospheric turbulent flows in the idealized planetary boundary layer, *J. Atmos. Sci., 30,* 1327–1339, 1973.

Simons, T. J., Verification of seasonal stratification models, report, Inst. of Meteorol. and Oceanogr., Univ. of Utrecht, Netherlands, 1980.

So, R. M. C., A turbulent velocity scale for curved shear flows, *J. Fluid Mech., 70,* 37–57, 1975.

So, R. M. C., and G. L. Mellor, Experiments on convex curvature effects in turbulent boundary layers, *J. Fluid Mech., 60,* 43–63, 1973.

So, R. M. C., and G. L. Mellor, Experiments on turbulent boundary layers on concave wall, *Aeronaut. Q. XXVI,* 25–40, 1975.

Sommeria, B., and J. W. Deardorff, Subgrid scale condensation in cloud models, *J. Atmos. Sci., 34,* 344–355, 1977.

Sun, W.-Y., and Y. Ogura, Modeling the evolution of the convective planetary boundary layer, *J. Atmos. Sci., 37,* 1558–1572, 1980.

Tennekes, H., and J. L. Lumley, *A First Course in Turbulence,* 293 pp., MIT Press, Cambridge, Mass., 1972.

Uberoi, M. S., Effect of wind-tunnel contraction on free stream turbulence, *J. Aeronaut. Sci., 23,* 754–764, 1956.

Uberoi, M. S., Equipartition of energy and local isotropy in turbulent flows, *J. Appl. Phys., 18,* 1165–1170, 1957.

Weatherly, G. L., and P. J. Martin, On the structure and dynamics of the ocean bottom boundary layer, *J. Phys. Oceanogr., 8,* 557–570, 1978.

Wieringa, J., A reevaluation of the Kansas Mast influence on measurements of stress and anemometer overspeeding, *Boundary Layer Meteorol., 18,* 411–430, 1980.

Willis, G. E., and J. W. Deardorff, A laboratory model of the unstable planetary boundary layer, *J. Atmos. Sci., 31,* 1297–1307, 1974.

Wolfstein, M., On the length-scale of turbulence equation, *Isr. J. Technol., 8,* 87–99, 1970.

Worthem, S., and G. L. Mellor, A turbulence of closure model applied to the upper tropical ocean, *Deep Sea Res.,* Gate Suppl. I, *26,* 237–272, 1980.

Wyngaard, J. C., Modeling the planetary boundary layer—Extension to the stable case, *Boundary Layer Meteorol., 9,* 441–460, 1975.

Yajnik, K. S., Asymptotic theory of turbulent shear flow, *J. Fluid Mech., 42,* 411–427, 1970.

Yamada, T., A numerical experiment on pollutant dispersion in a horizontally-homogeneous-atmospheric boundary layer, *Atmos. Environ., 11,* 1015–1024, 1977.

Yamada, T., A three-dimensional, second-order closure numerical model of mesoscale circulation in the lower atmosphere, *Topical Rep. ANL/RER-78-1,* 67 pp., Radiol. and Environ. Res. Div., Argonne Natl. Lab., Argonne, Ill., 1978*a*.

Yamada, T., A three-dimensional numerical study of complex atmospheric circulations produced by terrain, in *Proceedings: Conference on Sierra Nevada Meteorology,* pp. 61–67, American Meteorological Society, Boston, Mass., 1978*b*.

Yamada, T., An application of a three-dimensional, simplified second moment closure numerical model to study atmospheric effects of a large cooling-pond, *Atmos. Environ., 13,* 693–704, 1979.

Yamada, T., A numerical simulation of nocturnal drainage flow, *J. Meteorol. Soc. Jpn., 59,* 108–122, 1981.

Yamada, T., A numerical model study of turbulent airflow in and above a forest canopy, *J. Meteorol. Soc. Jpn., 60,* 439–454, 1982*a*.

Yamada, T., Simulations of nocturnal drainage flows by a q^2-l turbulence closure model, *J. Atmos. Sci.*, in press, 1982*b*.

Yamada, T., and G. L. Mellor, A simulation of the Wangara atmospheric boundary layer data, *J. Atmos. Sci., 32,* 2309–2329, 1975.

Yamada, T., and G. L. Mellor, A numerical simulation of the BOMEX data using a turbulence closure model coupled with ensemble cloud relations, *Q. J. R. Meteorol. Soc., 105,* 915–944, 1979.

Yokoyama, O., M. Gammo, and S. Yamamoto, On the turbulence quantities in the atmospheric mixing layer, *J. Meteorol. Soc. Jpn. 55,* 182–192, 1977.

Young, M. B. O., E. Y. Hsu, and R. L. Street, Air-water interaction: The nature of turbulent heat mass and momentum transfer mechanisms in the air boundary layer, *Tech. Rep. 163,* Dep. of Civ. Eng., Stanford Univ., Stanford, Calif., 1973.

Zeman, O., and J. L. Lumley, Modeling buoyancy driven mixed layers, *J. Atmos. Sci., 33,* 1974–1988, 1976.

(Received February 9, 1981;
accepted May 10, 1982.)